QUASIHALO ORBITS ASSOCIATED WITH LIBRATION POINTS

G. GÓMEZ
Departament de Matemàtica Aplicada i Anàlisi, Universitat de Barcelona
Gran Via 585, 08007 Barcelona, Spain
J. MASDEMONT
Departament de Matemàtica Aplicada I, Universitat Politècnica de Catalunya
E.T.S.E.I.B., Diagonal 647, 08028 Barcelona, Spain
C. SIMÓ
Departament de Matemàtica Aplicada i Anàlisi, Universitat de Barcelona
Gran Via 585, 08007 Barcelona, Spain

Abstract

Quasihalo orbits are Lissajous trajectories librating about the well known halo orbits. The main feature of these orbits is that they keep an exclusion zone in the same way that halo orbits do. As a result, the knowledge of this type of orbit, gives more flexibility to the mission analysis design about collinear libration points of any pair of primaries in the solar system. This paper is devoted to the semianalytical computation of quasihalo orbits in the Circular Restricted Three Body Problem by means of an ad hoc Lindstedt–Poincaré method. The study of the practical convergence of the procedure and the extension of the orbits to suitable locations in the solar system using JPL ephemerides is also discussed.

Key words: Circular restricted three body problem, halo orbits, quasi–periodic orbits, Lissajous orbits, quasihalo orbits, Lindstedt–Poincaré, Floquet theory.

1 INTRODUCTION

Halo orbits in the circular restricted three body problem (RTBP) are spatial periodic solutions which bifurcate from the planar Lyapunov orbits around the collinear libration points at a given amplitude (see [17], [18], [39]). At the bifurcation, due to the symmetry of the equations of motion, two families of halo orbits appear. These two families are symmetric with respect to the (x, y) plane and, according to [31], are called families of halo orbits of class I and II. Each one is an uniparametric family of orbits which can be parametrized by the z–amplitude (at least locally). For small z–amplitudes the period of the halo orbits is, roughly, one half of the period of the primaries.

Lissajous type trajectories around the collinear equilibrium points have been considered in the trajectory design of astrodynamic missions (see [7], [8], [21], [33], [35]). Recently, semianalytical computations of normal forms in Hamiltonian systems, provide the global description and a systematic study of all the possible librating trajectories in a large vicinity of the collinear equilibrium points (see [12], [16], [24], [26], [28]). These studies give a neat description of the libration orbits about the collinear equilibrium points: Lyapunov planar and vertical periodic orbits, the two families of periodic halo orbits, nonlinear Lissajous orbits around the libration point and nonlinear Lissajous orbits filling 2D tori around the halo orbits, the so called quasihalo orbits, give the basic structure of the center manifold associated with the collinear libration points.

Richardson [30] introduced, for the RTBP, reference systems and a formulation suitable for the study of the motion around the collinear libration points. Both are specially useful for the analytical computation of halo and Lissajous orbits about the libration points by means of the Lindstedt–Poincaré procedure. With the help of ad hoc algebraic manipulators, these orbits can be obtained up to a high order in a fast way, giving very accurate solutions (see [11], [12], [24]).

In this paper we present a semianalytical method, based on a Lindstedt–Poincaré (from now on LP) procedure (see [10], [29]), to compute the 2D tori around a halo orbit. We will compute series expansions for its coordinates depending on three parameters (one amplitude and two phases). Once the values of these parameters are fixed, we get an orbit on the torus. Halo orbits are identified by the *normalized z–amplitude*, that is, the amplitude of the first harmonic in the expansion of the z variable, expressed in normalized coordinates (see later). For small amplitudes they can also be uniquely identified by the frequency. Given a halo orbit of frequency ω, the series obtained for any one of the coordinates, $x(t)$, $y(t)$ and $z(t)$, of a quasihalo orbit, are of the form

$$\sum_i \left(\sum_{k,m} c_i^{km} \begin{matrix} \cos \\ \sin \end{matrix} \ (k(\omega t + \phi_1) + m(\nu t + \phi_2)) \right) \gamma^i.$$

These expansions depend on two frequencies, ω and ν, and one amplitude, γ. This amplitude is related to the size of the torus around the "base" halo orbit which is taken as backbone. Later on we will comment on possible "normalizations" in the definition of γ. The frequency ν is the second natural frequency of the torus, and it is close to the normal frequency around the base halo orbit.

Strictly speaking, these series are asymptotic but divergent everywhere. The high order resonances, which produce the small stochastic zones associated with the divergence, show up only when the expansion is carried up to the order of the resonances. Their effect, for moderate time intervals, is rather small. The computed series have been usually truncated at order 25 (some checks are carried out at order 35), and several tests have been done in order to compute a "practical" radius of convergence in terms of γ and depending on the base halo orbit.

Extending the RTBP to the real solar system, taking for instance the Sun and the Earth–Moon barycentre as primaries, halo orbits are no longer periodic but quasiperiodic (see [25], [27]). This is due to the fact that the perturbations of the bodies of the solar system act in a quasiperiodic way, at least for a moderate time span of a few centuries. Lissajous orbits, both around the equilibrium point and the quasihalo ones, are already quasiperiodic in the RTBP. The perturbations of the other bodies of the solar system in this case add more frequencies to the trajectory. In order to extend the orbits obtained for the RTBP, the paper ends with a numerical procedure that obtains real orbits using JPL ephemerides. For this purpose, the quasihalo orbits given by the expansions are taken as initial seeds of the procedure. An accurate initial seed has the advantage that the corrections to be performed are small.

The methodology developed in this paper can be applied to any family of halo orbits around any collinear equilibrium point of a RTBP (e.g.: Sun–Jupiter, Sun–Mars, Earth–Moon, Sun–Earth, ...). Recently, many missions have been proposed to take advantage of the growing scientific interest in the region near the libration points in the Sun–Earth system. The knowledge of the phase space around the libration points gives much more flexibility to the design process, at the same time that more complex missions can be envisioned. In particular, the characteristics of quasihalo orbits seem appropiate to the maintenance of a cluster of spacecrafts in formation around the equilibrium points at low cost.

In this paper we present the computations done for the Sun–Earth+Moon and Earth–Moon systems around the libration points L_1 and L_2. The L_1 point in the Sun–Earth+Moon system is located between the two primaries at approximately 1 500 000 km from the Earth. Halo type orbits around this point give suitable sites to locate spacecrafts devoted to the study of the Sun. They were first used in 1978 by the NASA mission ISEE-3. The SOHO spacecraft, launched in 1996, is using this kind of solution as a nominal orbit too (see [9], [13], [14], [15], [23], [32], [34]), and the GENESIS mission (see [19]) is currently planned to be launched the year 2001.

Halo orbits located around the L_2 equilibrium point (behind the small primary) in the Sun–Earth+Moon system (also at roughly 1 500 000 km from the Earth) are of interest in the studies of the geomagnetospheric tail at large geocentric distances and the cosmic background radiation (Primordial Structures Investigation (PSI) mission). In addition to PSI, other missions like

FIRE and Relict 2 have been considered but were not funded. The European Space Agency is considering two missions to L_2: FIRST and Plank. Furthermore, the Next Generation Space Telescope (NGST), which is the follow–on to the Hubble Telescope, is considering an L_2 libration point orbit. The same kind of orbits, but in the Earth–Moon system, can be useful for the communications with a translunar base.

2 HALO ORBITS AS EQUILIBRIUM POINTS

In a first approach, and to present the key ideas in a simple way, we consider as a model of motion for the spacecraft the circular restricted three body problem, with the Sun as the big primary located on the positive x axis and the Earth–Moon barycentre as the small primary lying on the same axis on the negative side. The value of the RTBP mass parameter that has been used in the computations is the one obtained using the values of the masses of the Sun, Earth and Moon given by the JPL ephemerides DE403, and is equal to $3.040423398444176 \cdot 10^{-6}$ for the Sun–Earth+Moon system and to $1.215058191870689 \cdot 10^{-2}$ for the Earth–Moon system. Of course, not all these figures are meaningful, but these are the concrete numerical values used in the present paper.

In order to apply the LP method to compute the two dimensional tori around a halo orbit, it is convenient to perform a change of variables which transforms the halo orbit to an equilibrium point of the equations of motion. Then, orbits librating around the equilibrium point in the new coordinates correspond to orbits librating around the halo orbit in the original ones.

As one can guess, the halo orbit used as backbone becomes an equilibrium point via a time dependent transformation. In the new variables the equations of motion are non autonomous, and the complexity of the problem increases, but, since halo orbits are periodic, the time dependence in the new equations of motion will be also periodic. The expansions of the equations, which must be done in the LP procedure, will have periodic coefficients too. Moreover, the computation of the libration orbits around the equilibrium point of these new equations cannot be done via the LP method unless the linear part has constant coefficients. This requirement is fulfilled via a Floquet change of variables. In this section we are going to show how the previous mentioned transformation and the Floquet change of variables are implemented.

The equations of motion of the RTBP where the small primary, of mass μ, is located at $(\mu-1,0,0)$ and the big one, with mass $1-\mu$, at $(\mu,0,0)$ are

$$\ddot{X}_1 - 2\dot{X}_2 = \Omega_{X_1}, \quad \ddot{X}_2 + 2\dot{X}_1 = \Omega_{X_2}, \quad \ddot{X}_3 = \Omega_{X_3},$$

$$\Omega(X_1,X_2,X_3) = \frac{1}{2}(X_1^2+X_2^2) + \frac{1-\mu}{r_1} + \frac{\mu}{r_2},$$

where $X=(X_1,X_2,X_3)$ are the usual *adimensional synodical coordinates* with the origin at the centre of mass and $r_1^2=(X_1-\mu)^2+X_2^2+X_3^2$, $r_2^2=(X_1-\mu+1)^2+X_2^2+X_3^2$. By introducing $P_1=\dot{X}_1-X_2$, $P_2=\dot{X}_2+X_1$ and $P_3=\dot{X}_3$, the Hamiltonian is

$$\mathcal{H} = \frac{1}{2}(P_1^2+P_2^2+P_3^2) + X_2P_1 - X_1P_2 + \frac{1}{2}(X_1^2+X_2^2) - \Omega\,.$$

We denote the collinear equilibrium points by L_1, L_2 and L_3. They are located between the primaries, in the negative part of the X_1 axis, and in the positive part of the X_1 axis, respectively. A preliminary change of coordinates allows us to expand the equations of motion in power series around any of the mentioned equilibria (see [12], [31]). Denoting by $x=(x_1,x_2,x_3)$ the adimensional coordinates around a selected equilibrium point, L_i, the change of variables to a new ones, denoted as *normalized coordinates*, is given by

$$X_1 = \mp\psi x_1 + \mu + a, \quad X_2 = \mp\psi x_2, \quad X_3 = \psi x_3,$$

where the upper sign corresponds to L_1 and L_2, whilst the lower one corresponds to L_3. The value of a is, respectively, $-1+\psi$, $-1-\psi$ and ψ for L_1, L_2 and L_3, where ψ is the distance from the equilibrium point to the nearest primary. It can be computed solving the corresponding Euler's quintic equation. For instance, for L_1 we have

$$\psi^5 - (3-\mu)\psi^4 + (3-2\mu)\psi^3 - \mu\psi^2 + 2\mu\psi - \mu = 0,$$

for L_2

$$\psi^5 + (3-\mu)\psi^4 + (3-2\mu)\psi^3 - \mu\psi^2 - 2\mu\psi - \mu = 0,$$

and for L_3

$$\psi^5 + (2+\mu)\psi^4 + (1+2\mu)\psi^3 - (1-\mu)\psi^2 - 2(1-\mu)\psi - (1-\mu) = 0.$$

Using these coordinates and series expansions around the origin, the equations of motion can be written in the form (see [31])

$$\begin{aligned} \ddot{x}_1 - 2\dot{x}_2 - (1+2c_2)x_1 &= \frac{\partial}{\partial x_1}\sum_{n\geq 3} c_n\rho^n P_n\left(\frac{x_1}{\rho}\right), \\ \ddot{x}_2 + 2\dot{x}_1 + (c_2-1)x_2 &= \frac{\partial}{\partial x_2}\sum_{n\geq 3} c_n\rho^n P_n\left(\frac{x_1}{\rho}\right), \\ \ddot{x}_3 + c_2x_3 &= \frac{\partial}{\partial x_3}\sum_{n\geq 3} c_n\rho^n P_n\left(\frac{x_1}{\rho}\right), \end{aligned} \tag{1}$$

where $\rho^2 = x_1^2 + x_2^2 + x_3^2$, P_n is the Legendre polynomial of degree n and c_n are constants, depending only on μ, defined by

$$\begin{aligned} c_n &= \tfrac{1}{\psi^3}\left[\mu + (-1)^n(1-\mu)\left(\tfrac{\psi}{1-\psi}\right)^{n+1}\right], && \text{in the } L_1 \text{ case,} \\ c_n &= \tfrac{(-1)^n}{\psi^3}\left[\mu + (1-\mu)\left(\tfrac{\psi}{1+\psi}\right)^{n+1}\right], && \text{in the } L_2 \text{ case,} \\ c_n &= \tfrac{(-1)^n}{\psi^3}\left[1-\mu + \mu\left(\tfrac{\psi}{1+\psi}\right)^{n+1}\right], && \text{in the } L_3 \text{ case.} \end{aligned}$$

The equations (1) are the starting point for our computations. Since a great amount of symbolic manipulation must be done, it is convenient to write down the right hand part of these equations using functions which can be computed (and stored) in a fast and easy way. Following [12] this is done by introducing the functions

$$T_n(x_1,x_2,x_3) = \rho^n P_n\left(\frac{x_1}{\rho}\right) \quad \text{and} \quad R_{n-1}(x_1,x_2,x_3) = \frac{1}{x_2}\frac{\partial T_{n+1}}{\partial x_2}.$$

It is not difficult to see that T_n and R_n are polynomials of degree n satisfying also

$$R_{n-1}(x_1,x_2,x_3) = \frac{1}{x_3}\frac{\partial T_{n+1}}{\partial x_3} \quad \text{and} \quad \frac{\partial T_{n+1}}{\partial x_1} = (n+1)T_n.$$

Using T_n and R_n, the equations become

$$\begin{aligned} \ddot{x}_1 - 2\dot{x}_2 - (1+2c_2)x_1 &= \sum_{n\geq 2} c_{n+1}(n+1)T_n, \\ \ddot{x}_2 + 2\dot{x}_1 + (c_2-1)x_2 &= x_2\sum_{n\geq 2} c_{n+1}R_{n-1}, \\ \ddot{x}_3 + c_2x_3 &= x_3\sum_{n\geq 2} c_{n+1}R_{n-1}, \end{aligned} \tag{2}$$

where R_n and T_n can be obtained using the recurrences that follow from the properties of the Legendre polynomials,

$$\begin{aligned} T_n(x_1,x_2,x_3) &= \left(2-\frac{1}{n}\right)x_1T_{n-1}-\left(1-\frac{1}{n}\right)\rho^2T_{n-2}, \\ R_n(x_1,x_2,x_3) &= \frac{2n+3}{n+2}x_1R_{n-1}-\frac{2n+2}{n+2}T_n-\frac{n+1}{n+2}\rho^2R_{n-2}, \end{aligned}$$

starting with $T_0=1$, $T_1=x_1$, $R_0=-1$ and $R_1=-3x_1$.

The above equations of motion can also be put in Hamiltonian form. Denoting by $p_{x_1}=\dot{x}_1-x_2$, $p_{x_2}=\dot{x}_2+x_1$ and $p_{x_3}=\dot{x}_3$, the corresponding Hamiltonian is

$$H=\frac{1}{2}(p_{x_1}^2+p_{x_2}^2+p_{x_3}^2)+x_2p_{x_1}-x_1p_{x_2}-\sum_{n\geq 2}c_n\rho^nP_n\left(\frac{x_1}{\rho}\right).$$

We remark, because it is useful for numerical checks that involve the computation of the energy, that in the above formula the following more compact expression holds

$$\sum_{n\geq 2}c_n\rho^nP_n\left(\frac{x_1}{\rho}\right)=\psi^{-2}\left(\frac{1-\mu}{r_1}+\frac{\mu}{r_2}-\frac{1-\mu}{1-\psi}(1-\frac{\psi}{1-\psi}x_1)-\frac{\mu}{\psi}(1+x_1)\right),$$

where, now, $r_1^2=(1-\psi)^2\left[1+\frac{2\psi}{1-\psi}x_1+\left(\frac{2\psi}{1-\psi}\right)^2\rho^2\right]$ and $r_2^2=\psi^2[1-2x_1+\rho^2]$. The relation between the "adimensional synodical" Hamiltonian and the "normalized" one is $\mathcal{H}=\psi^2H-\frac{1}{2}(1-\mu-\psi)^2-\frac{1-\mu}{1-\psi}-\frac{\mu}{\psi}$.

Denoting by $x=(x_1,x_2,x_3,x_4,x_5,x_6)\equiv(x_1,x_2,x_3,\dot{x}_1,\dot{x}_2,\dot{x}_3)$, the equations of motion (2) can be written in compact form as $\dot{x}=f(x)$. Assume now that $\bar{x}(t)=(\bar{x}_1(t),\bar{x}_2(t),\bar{x}_3(t),\dot{\bar{x}}_1(t),\dot{\bar{x}}_2(t),\dot{\bar{x}}_3(t))$ is a halo orbit solution of the equations (2). The time dependent change of variables $x=z+\bar{x}$ transforms $\dot{x}=f(x)$ into $\dot{z}+\dot{\bar{x}}=f(z+\bar{x})$. Expanding $f(z+\bar{x})$ in power series around the halo orbit we get

$$f(z+\bar{x})=f(\bar{x})+A(\bar{x})z+g(z,\bar{x}),$$

where $A(\bar{x})$ is a time dependent matrix, and $g(z,\bar{x})$ is a function whose Taylor series expansion in powers of z_i, $i=1\dots 6$, starts at order two and it has time dependent coefficients. Both A and g can be obtained by symbolic manipulation.

Since the halo orbit is a solution of the initial equations, we have $\dot{\bar{x}}=f(\bar{x})$, and so

$$\dot{z}=A(\bar{x}(t))z+g(z,\bar{x}(t)), \tag{3}$$

where the linear part of these equations, $\dot{z}=A(\bar{x}(t))z$, gives rise to the variational equations on the halo orbit.

The fact that the halo orbit is periodic implies that the time dependence in (3) is also periodic. In this way, the halo orbit $\bar{x}(t)$ can be seen as a function of an angle Φ_1, $\bar{x}(\Phi_1)$, where $\Phi_1=\omega t+\phi_1$, ω is the frequency of the halo orbit, and ϕ_1 is a phase. If T denotes the period of the halo orbit then $T\omega=2\pi$.

In order to apply the LP procedure, it is advisable that the matrix A of (3) be constant. As its time dependence is periodic, it can be removed via a Floquet change of coordinates. This is a linear change of variables with periodic coefficients that we will denote by $z=Py$, where $P=P(\Phi_1)$ is a periodic matrix.

Introducing $z=Py$ in (3) we get $\dot{P}y+P\dot{y}=APy+g(Py,\Phi_1)$, that is,

$$\dot{y}=(P^{-1}AP-P^{-1}\dot{P})y+P^{-1}g(Py,\Phi_1).$$

The matrix P is computed solving $\dot{P} = AP - PB$, where B is known as the Floquet matrix. B is a constant matrix which is a logarithm of the monodromy matrix of $\dot{z} = A(\bar{x}(t))z$ divided by the period T (see [6]). In this way, equations (3) become

$$\dot{y} = By + Qg(Py, \Phi_1), \tag{4}$$

where $Q = P^{-1}$. In the present problem, the matrix B, after a suitable change of basis, can be simplified to

$$B = \begin{pmatrix} 0 & 0 & 0 & 1 & 0 & 0 \\ 0 & 0 & 0 & 0 & 1 & 0 \\ 0 & 0 & 0 & 0 & 0 & 1 \\ b_{41} & 0 & b_{43} & 0 & b_{45} & 0 \\ 0 & 0 & 0 & b_{54} & 0 & b_{56} \\ b_{61} & 0 & b_{63} & 0 & b_{65} & 0 \end{pmatrix}. \tag{5}$$

Note that the final equations (4) can be obtained from the original ones (2) using the linear change of variables

$$x = P(\Phi_1)y + \bar{x}(\Phi_1). \tag{6}$$

Next we are going to show the main points of the computation and implementation of this transformation.

2.1 Computational aspects

In order to get equation (4), we must know the matrix $P(\Phi_1)$, the halo orbit $\bar{x}(\Phi_1)$, and the constant Floquet matrix B.

Taking into account that the final goal of the procedure is to obtain Lissajous orbits around a halo orbit expanded as a series, and that the time dependence we are dealing with is periodic, all the periodic functions and coefficients are handled using Fourier series up to a certain order. Initially, one must compute the halo orbit. This can be done either numerically or semianalytically. Both procedures have been implemented in our computations and the possibilities will be discused in what follows.

One can compute a halo orbit using a numerical procedure for computing families of periodic orbits and then to perform a Fourier analysis of its coordinates. We can also use a Lindstedt–Poincaré procedure for the computation of the family of halo orbits and then determine the desired orbit in the family (see [12]). Both approaches give us the halo orbit as Fourier series that can be chosen of cosinus type for the x_1 and x_3 components and of sinus type for x_2, due to the symmetries of the problem. This is,

$$\bar{x}_1 = \sum_k \bar{x}_{1k} \cos k\Phi_1, \quad \bar{x}_2 = \sum_k \bar{x}_{2k} \sin k\Phi_1, \quad \bar{x}_3 = \sum_k \bar{x}_{3k} \cos k\Phi_1.$$

The next step is to compute the matrix B. This is somewhat longer. As we have said, the matrix B is a logarithm of the monodromy matrix around the halo orbit divided by the period T of the halo orbit. The monodromy matrix can be obtained numerically integrating the variational equations on the halo orbit at the same time that we compute the halo orbit numerically. In case that the Fourier expansions for the coordinates of a halo orbit are already known, for instance if we use a LP procedure for the halo orbits, it can be obtained as well integrating only the variational equations $\dot{Z} = A(\Phi_1)Z$, where $A(\Phi)$ can be computed using these expansions. Of course $Z(0) = I$. This second approach is more cumbersome to carry out in practice since the semianalytical computation of the matrix $A(\Phi_1)$ must be done using both the change of coordinates, $x = z + \bar{x}$, and the truncated Fourier series for the halo orbit. Using symbolic manipulation, the linear part of the resulting equations, which gives us $A(\Phi_1)$, can be solved. In order to check the results and to compute them efficiently, we use the fact that, due to the symmetries of the equations, the matrix A has its entries, $a_{ij}(\Phi_1)$, of cosinus (resp. sinus) type when $i+j$ is even (resp. odd).

Assume that the monodromy matrix, $M = Z(T)$, is available. To compute its logarithm, first we put it in Jordan form via a change of basis V. This is, $M_J = V^{-1}MV$, where for small halo orbits the structure that we have is

$$M_J = \left(\begin{array}{cc|cc|cc} \lambda & & & & & \\ & \lambda^{-1} & & & 0 & \\ \hline & & 1 & \varepsilon & & \\ & & 0 & 1 & & \\ \hline & 0 & & & \cos\Gamma & -\sin\Gamma \\ & & & & \sin\Gamma & \cos\Gamma \end{array} \right).$$

The logarithm of this matrix divided by the period is

$$F_J = \frac{1}{T} \left(\begin{array}{cc|cc|cc} \log\lambda & & & & & \\ & -\log\lambda & & & 0 & \\ \hline & & 0 & \varepsilon & & \\ & & 0 & 0 & & \\ \hline & 0 & & & 0 & -\Gamma \\ & & & & \Gamma & 0 \end{array} \right),$$

and the Floquet matrix, F, is obtained undoing the change V, so $F = (f_{ij}) = VF_JV^{-1}$. In order to put the Floquet matrix in the simplified form, B, that appears in (5), we must perform another change of variables, S, so $B = SFS^{-1}$. The explicit expression of S in terms of the components of $F = (f_{ij})$ is

$$S = \begin{pmatrix} 1 & 0 & 0 & 0 & 0 & 0 \\ 0 & 1 & 0 & 0 & 0 & 0 \\ 0 & 0 & 1 & 0 & 0 & 0 \\ 0 & f_{12} & 0 & f_{14} & 0 & f_{16} \\ f_{21} & 0 & f_{23} & 0 & f_{25} & 0 \\ 0 & f_{32} & 0 & f_{34} & 0 & f_{36} \end{pmatrix}.$$

Finally, the Floquet change of basis is obtained by integrating $\dot{\bar{P}} = A\bar{P} - \bar{P}F$, from $t = 0$, until $t = T$ and taking $\bar{P}(0) = I$. The entries of $\bar{P}$ are periodic functions of period T. To get the periodic matrix P appearing in (6), which gives the final equations (4), $P = \bar{P}S^{-1}$ and its inverse $Q = P^{-1} = S\bar{P}^{-1}$ are stored in a mesh of points in order to perform a Fourier analysis of its components. Due to symmetry, the respective components p_{ij} and q_{ij} of P and Q are of cosinus (resp. sinus) type when $i+j$ is even (resp. odd).

3 THE LINDSTEDT–POINCARÉ PROCEDURE

In this section we are going to explain how we compute the quasihalo orbits of the equations (4) by means of a LP method.

First of all, we note that the equations $\dot{x} = f(x)$ of the RTBP at the equilibrium point have

$f_1 = f_2 = f_3 = 0$ and so in (4), $g_1 = g_2 = g_3 = 0$. The system (4) can be written as

$$\begin{pmatrix} \dot y_1 \\ \dot y_2 \\ \dot y_3 \\ \dot y_4 \\ \dot y_5 \\ \dot y_6 \end{pmatrix} = \left(\begin{array}{ccc|ccc} & & & 1 & & \\ & 0 & & & 1 & \\ & & & & & 1 \\ \hline b_{41} & 0 & b_{43} & 0 & b_{45} & 0 \\ 0 & 0 & 0 & b_{54} & 0 & b_{56} \\ b_{61} & 0 & b_{63} & 0 & b_{65} & 0 \end{array}\right) \begin{pmatrix} y_1 \\ y_2 \\ y_3 \\ y_4 \\ y_5 \\ y_6 \end{pmatrix} + Q \begin{pmatrix} 0 \\ 0 \\ 0 \\ g_4(Py) \\ g_5(Py) \\ g_6(Py) \end{pmatrix}, \tag{7}$$

where the functions g depend periodically on time (both directly and through P).

Using the first three equations we obtain,

$$\dot y_j \;=\; y_{j+3} + \sum q_{j,i+3} g_{i+3}(Py), \;\; j = 1, 2, 3, \tag{8}$$

where in all the sums, from now on and unless otherwise stated, i runs from 1 to 3. Taking derivatives with respect to time we have, for $j = 1, 2, 3$,

$$\dot y_{j+3} \;=\; \ddot y_j - \sum \dot q_{j,i+3} g_{i+3}(Py) - \sum q_{j,i+3} \dot g_{i+3}(Py).$$

Inserting these derivatives into the last three equations of (7) and making use of (8), we get

$$\begin{aligned} \ddot y_1 - b_{41} y_1 - b_{43} y_3 - b_{45} \dot y_2 &= -b_{45} \sum q_{2,i+3} g_{i+3}(Py) + \\ &\quad \sum \left(\dot q_{1,i+3} g_{i+3}(Py) + q_{1,i+3} \dot g_{i+3}(Py) + q_{4,i+3} g_{i+3}(Py)\right), \\ \ddot y_2 - b_{54} \dot y_1 - b_{56} \dot y_3 &= -\sum \left(b_{54} q_{1,i+3} + b_{56} q_{3,i+3}\right) g_{i+3}(Py) + \\ &\quad \sum \left(\dot q_{2,i+3} g_{i+3}(Py) + q_{2,i+3} \dot g_{i+3}(Py) + q_{5,i+3} g_{i+3}(Py)\right), \\ \ddot y_3 - b_{61} y_1 - b_{63} y_3 - b_{65} \dot y_2 &= -b_{65} \sum q_{2,i+3} g_{i+3}(Py) + \\ &\quad \sum \left(\dot q_{3,i+3} g_{i+3}(Py) + q_{3,i+3} \dot g_{i+3}(Py) + q_{6,i+3} g_{i+3}(Py)\right), \end{aligned} \tag{9}$$

where the left hand side contains the linear part and the right hand one the higher order terms. Note that in these equations Py, which appears in the functions g_j, still contains the variables y_4, y_5, y_6, implying that equations (9) are coupled with equations (8).

Since the goal of a LP procedure is to get a formal series solution of equations (4), we can proceed doing the following steps, that will be explained later in more detail. Here, "order" denotes the order with respect to the parameter γ.

- Start by computing the solution of the linear part of (9). As we will see, this gives us the order one of the series expansion of y_1, y_2, y_3.
- Use (8) to determine y_4, y_5, y_6 up to order one. Up to this order we have $y_4 = \dot y_1$, $y_5 = \dot y_2$, $y_6 = \dot y_3$.
- Assume that y_1, y_2, y_3, y_4, y_5, y_6 have been determined up to a certain order $n-1$.
- Take (9) and apply the LP procedure to determine the order n of y_1, y_2, y_3. We note that since the right hand side part of (9) begins with quadratic terms in Py, for this step we only need y_1, y_2, y_3, y_4, y_5, y_6 up to order $n-1$, to equate the terms of order n of both sides.
- Use (8) again to determine the terms of order n of y_4, y_5, y_6. For this purpose we need y_1, y_2, y_3 up to order n, computed previously, and y_4, y_5, y_6 up to order $n-1$, computed in the preceding iteration.

- Repeat the last three steps up to a desired order N (to be defined later).

Taking into account the type of series (sinus or cosinus) of the halo orbit $\bar{x}$ that determine the type of the entries of P and relation (6), we get that y_1, y_3 and y_5 will be cosinus type series whilst y_2, y_4 and y_6 will be of sinus type. Then series expansions for y_j, $j = 1, ..., 6$, are searched in the following way,

$$y_j(t) \quad = \quad \sum_{i=1}^{\infty} \left(\sum_{k,m} y_{j,i}^{k,m} \begin{matrix} \cos \\ \sin \end{matrix} \left(k\Phi_1 + m\Phi_2 \right) \right) \gamma^i. \tag{10}$$

For the angles Φ_1 and Φ_2 we use the expressions,

$$\Phi_1 = \omega t + \phi_1, \qquad \Phi_2 = \nu t + \phi_2,$$

where Φ_1 is the same as in the halo orbit, this is, ω is the frequency of the backbone halo orbit. The frequency ν is related to the motion of the Lissajous orbit around the halo one. Due to the nonlinear character of equations (7), it cannot be kept fixed. Specifically, ν depends on the amplitude γ which essentially measures the displacement from the quasihalo orbit to the selected base halo one. It must be expanded in the form

$$\nu = \sum_{i=0}^{\infty} \nu_i \gamma^i. \tag{11}$$

Giving arbitrary values to the phases ϕ_1, ϕ_2 and to the amplitude γ (this one inside the range of "convergence" which will be discused later), we obtain all the quasihalo orbits about a halo orbit which have one of the fundamental frequencies equal to the one of the halo selected. At this point we notice that $\gamma = 0$ implies $y = 0$ and due to (6), the solution that we get is the halo orbit. Moreover, due to the autonomous character of the RTBP, one can fix one of the phases equal to zero and, by varying γ and the other phase, the same set of solutions is obtained.

Assuming the halo orbit expanded as an infinite Fourier series, the range for k in (10) goes from 0 to ∞. During the procedure only y terms with $|m| \leq i$ and $m \equiv i \pmod 2$ show up. Also only terms ν_i with i even appear. Since the expansions of the halo orbit are truncated to l harmonics, only terms with $k \leq l$ are kept in the expansions. Moreover when $k = 0$, changing the sign of the coefficient if necessary, only terms with $m \geq 0$ are kept. All these facts have been taken into account in the semianalytical implementation in order to save computing time and storage.

Of course the sum with respect to i in (10) must be truncated at some value N, ($N \leq l$), which will be known as the *order* of the final expansion. At the n-th step of the procedure the terms with $i = n$ of the y variables are determined. We say that at this step we have the solution up to order n, meaning that if we insert formally the expressions that we have for y into (4), the expansions obtained for the residuals, which are of the same type as (10), are zero for all the terms with $k \leq l$ and $i \leq n$. This property is the first one to be checked once we have computed the approximate solution at order N.

3.1 Computation of the linear part

The linear part of (9) is

$$\begin{aligned} \ddot{y}_1 - b_{41}y_1 - b_{43}y_3 - b_{45}\dot{y}_2 &= 0, \\ \ddot{y}_2 - b_{54}\dot{y}_1 - b_{56}\dot{y}_3 &= 0, \\ \ddot{y}_3 - b_{61}y_1 - b_{63}y_3 - b_{65}\dot{y}_2 &= 0. \end{aligned} \tag{12}$$

A non trivial librating solution of these equations must be used to determine the coefficients of (10) with $i=1$. This is, we are looking for the expansions up to order one of $y_j,\ \ j=1,2,3$, that we denote by y_j^1. They are,

$$y_j^1(t)=\gamma\sum_{k,m} y_{j,1}^{k,m}\ {\cos \atop \sin}\ (k\Phi_1+m\Phi_2).$$

Since (12) does not depend on the halo frequency ω, we must take $y_{j,1}^{k,m}=0,\ \ j=1,2,3$, for $k\neq 0$. Taking into account the above mentioned restrictions on the index, only $y_{j,1}^{0,1},\ \ j=1,2,3$, remain as free coefficients. So, for all γ and ϕ_2, we must look for a non trivial solution of the form

$$y_j^1(t)=\gamma y_{j,1}^{0,1}\ {\cos \atop \sin}\ (\nu t+\phi_2).$$

When we require that these expressions satisfy (12) we find

$$\begin{pmatrix} -(b_{41}+\nu^2) & -b_{45}\nu & -b_{43} \\ b_{54}\nu & -\nu^2 & b_{56}\nu \\ -b_{61} & -b_{65}\nu & -(b_{63}+\nu^2) \end{pmatrix}\begin{pmatrix} y_{1,1}^{0,1} \\ y_{2,1}^{0,1} \\ y_{3,1}^{0,1}\end{pmatrix}=\begin{pmatrix} 0\\ 0\\ 0\end{pmatrix}.$$

Since we need a non trivial solution, we must select the value of $\nu\neq 0$ making the determinant of the former linear system equal to zero. This is easily found by solving,

$$\nu^4+(b_{65}b_{56}+b_{54}b_{45}+b_{41}+b_{63})\nu^2+b_{41}b_{63}-b_{43}b_{61}+b_{65}b_{56}b_{41}+b_{54}b_{45}b_{63}-b_{54}b_{65}b_{43}-b_{61}b_{45}b_{56}=0.$$

The root of this equation gives us the term ν_0 in the expansion of ν given by (11). (Remark: The value of ν_0 is equal to Γ/T where Γ is the value that appears in the matrix M_J and T is the period of the halo orbit). As the linear system is homogeneous, we have a free parameter in the determination of the coefficients $y_{j,1}^{0,1},\ \ j=1,2,3$. This freedom is related to the different possible "normalizations" in the definition of the parameter γ. We have selected γ to be the coefficient of $\cos(\nu t+\phi_2)$ in the Fourier expansion of y_3. This means that $y_{3,1}^{0,1}=1$, and in this way we have an unique solution for the linear part. Concerning the higher order terms, this choice implies $y_{3,n}^{0,1}=0$ for all $n>1$. Any other choice can be reduced to this one by a suitable redefinition of γ, a fact which is assured by using the implicit function theorem.

Now we have the expansions of y_1, y_2 and y_3 up to order one,

$$y_1^1(t)=\gamma y_{1,1}^{0,1}\cos(\nu_0 t+\phi_2),\quad y_2^1(t)=\gamma y_{2,1}^{0,1}\sin(\nu_0 t+\phi_2),\quad y_3^1(t)=\gamma y_{3,1}^{0,1}\cos(\nu_0 t+\phi_2).$$

Finally, using (8) we get the terms of y_4, y_5 and y_6 of order one. In this case we have $y_{4,1}^{k,m}=y_{5,1}^{k,m}=y_{6,1}^{k,m}=0$ for $k\neq 0$, and $y_{4,1}^{0,1}=-\nu_0 y_{1,1}^{0,1}$, $y_{5,1}^{0,1}=\nu_0 y_{2,1}^{0,1}$ and $y_{6,1}^{0,1}=-\nu_0 y_{3,1}^{0,1}$.

3.2 Computation of the higher order terms

To compute the higher order terms we proceed recursively. Assume that at a certain step we have $y_j,\ \ j=1,...,6$, determined up to order $n-1$ and ν up to order $n-2$ (resp. $n-3$) if $n-1$ is odd (resp. even) (in fact we can assume ν determined up to order $n-2$ since otherwise, when it is only determined up to order $n-3$, then $n-2$ is odd and $\nu_{n-2}=0$). The insertion of these known terms in the right hand side of (9) produces expansions which are completely known up to order n. Let us denote them by $\bar r_{1,n}^{k,m}$, $\bar r_{2,n}^{k,m}$ and $\bar r_{3,n}^{k,m}$. We note that they are series as the ones in (10), of cosinus, sinus and cosinus type respectively. Given the expansions of x_1, x_2 and x_3 up to order $n-1$, they can be computed via the change of variables (6), and using the recurrences for T_j and R_j which appear in the equations (2). We note that the series for x_1, x_2 and x_3 are the final goal of our computations and they are of the same type of y_1, y_2 and y_3, respectively.

The purpose of the first part of the n-th step is to equate terms of order n in both sides of (9). Up to now we have computed the order n of the right hand side; now we must compute the order n of the left hand one. This latter part is made of an unknown part of order n and a known one that must be determined and added to $\bar{r}$.

Let us denote by s any one of the y functions. The derivatives with respect to time, which appear in the left hand side of equations (9), can be computed by

$$\begin{aligned}\dot{s} &= \frac{\partial s}{\partial \Phi_1}\frac{d\Phi_1}{dt} + \frac{\partial s}{\partial \Phi_2}\frac{d\Phi_2}{dt} = \omega\frac{\partial s}{\partial \Phi_1} + \nu\frac{\partial s}{\partial \Phi_2}, \\ \ddot{s} &= \omega^2\frac{\partial^2 s}{\partial \Phi_1^2} + 2\omega\nu\frac{\partial^2 s}{\partial \Phi_1 \partial \Phi_2} + \nu^2\frac{\partial^2 s}{\partial \Phi_2^2},\end{aligned}$$

where we recall that ω is constant but ν is given by the series (11). Since any partial derivative of s is formally a series like the ones in (10), the products of ν by partial derivatives are series products. Moreover, ν^2 is also a series product which is of the same type as (11). The order n of a series product that appears in our computations is obtained multiplying the part of order j of a frequency type series (11) by the part of order $n-j$ of an expansion type series like (10) and then adding the results from $j = 0$ to $j = n-1$ (we note that the series like (10) have no zero order part).

When j ranges from $j = 1$ to $n-2$ in the products of ν by a partial derivative, there appear known terms. In a similar way, known terms appear in the computation of ν^2 which is used later when computing $\nu^2\frac{\partial^2 s}{\partial \Phi_2^2}$ for the same values of j. Let us assume that all these values are added to the corresponding $\bar{r}_1^n$, $\bar{r}_2^n$ and $\bar{r}_3^n$. When $j = 0$ or $j = n-1$, the following table summarizes the terms that we have for $\dot{s}$ and $\ddot{s}$. The symbol δ stands for Kronecker's delta.

j	$n-j$	$\dot{s}$	$\ddot{s}$
0	n	$\pm(k\omega + m\nu_0)s_n^{k,m}$	$-(k\omega + m\nu_0)^2 s_n^{k,m}$
$n-1$	1	$\pm\nu_{n-1}s_1^{0,1}\delta_{k,0}\delta_{m,1}$	$-2\nu_0\nu_{n-1}s_1^{0,1}\delta_{k,0}\delta_{m,1} - N_{n-1}^2 s_1^{0,1}\delta_{k,0}\delta_{m,1}$

In the table, the $\pm$ sign has to be taken $+$ (resp. $-$) if s is a sinus (resp. cosinus) series. N_{n-1}^2 represents the known part of ν^2 of order $n-1$, obtained by multiplying the parts of order j of ν with the ones of order $n-j-1$ from $j = 1$ to $n-2$. $s_j^{k,m}$ represents the term (k,m) of the part of order j of the series s.

We note that the term $N_{n-1}^2 s_1^{0,1}\delta_{k,0}\delta_{m,1}$ in the previous table is known. So, all the contributions coming from these terms in the second derivatives of the y series in the left hand side of (9) can be included in the series $\bar{r}$. From now on we denote by r_1^n, r_2^n and r_3^n the part of order n of the respective initial series, $\bar{r}$, updated with the known part of order n coming from the left hand side of equations (9). Following the usual notation, we refer to the individual terms by $r_{1,n}^{k,m}$, $r_{2,n}^{k,m}$ and $r_{3,n}^{k,m}$.

By equating the terms of order n in both sides of (9) we obtain the linear system

$$\begin{aligned}-\left(\Psi^2 + b_{41}\right)y_{1,n}^{k,m} - b_{45}\Psi y_{2,n}^{k,m} - b_{43}y_{3,n}^{k,m} - (2\nu_0 y_{1,1}^{0,1} + b_{45}y_{2,1}^{0,1})\nu_{n-1}\delta_{k,0}\delta_{m,1} &= r_{1,n}^{k,m}, \\ b_{54}\Psi y_{1,n}^{k,m} - \Psi^2 y_{2,n}^{k,m} + b_{56}\Psi y_{3,n}^{k,m} + (b_{54}y_{1,1}^{0,1} + b_{56}y_{3,1}^{0,1} - 2\nu_0 y_{2,1}^{0,1})\nu_{n-1}\delta_{k,0}\delta_{m,1} &= r_{2,n}^{k,m}, \\ -b_{61}y_{1,n}^{k,m} - b_{65}\Psi y_{2,n}^{k,m} - \left(\Psi^2 + b_{63}\right)y_{3,n}^{k,m} - (2\nu_0 y_{3,1}^{0,1} + b_{65}y_{2,1}^{0,1})\nu_{n-1}\delta_{k,0}\delta_{m,1} &= r_{3,n}^{k,m},\end{aligned}$$

where $\Psi = k\omega + m\nu_0$. It must be solved for the unknowns $y_{1,n}^{k,m}$, $y_{2,n}^{k,m}$, $y_{3,n}^{k,m}$ and ν_{n-1}.

When $(k,m)\neq(0,1)$ it becomes

$$\begin{pmatrix} -b_{41}-\Psi^2 & -b_{45}\Psi & -b_{43} \\ b_{54}\Psi & -\Psi^2 & b_{56}\Psi \\ -b_{61} & -b_{65}\Psi & -b_{63}-\Psi^2 \end{pmatrix} \begin{pmatrix} y_{1,n}^{k,m} \\ y_{2,n}^{k,m} \\ y_{3,n}^{k,m} \end{pmatrix} = \begin{pmatrix} r_{1,n}^{k,m} \\ r_{2,n}^{k,m} \\ r_{3,n}^{k,m} \end{pmatrix}, \tag{13}$$

from where we get $y_{1,n}^{k,m}$, $y_{2,n}^{k,m}$ and $y_{3,n}^{k,m}$. We note that the case $(k,m)=(0,0)$ gives us a singular matrix, but it is easily solved taking $y_{2,n}^{0,0}=0$, since r_2 is a sinus type series and so $r_{2,n}^{0,0}=0$.

When $(k,m)=(0,1)$ (this only happens when n is odd) the matrix of (13) is singular since in the computations of the first order part we selected ν_0 in that way. But in this case we have the additional contribution of ν_{n-1} giving

$$\begin{pmatrix} -b_{41}-\nu_0^2 & -b_{45}\nu_0 & -b_{43} & -2\nu_0 y_{1,1}^{0,1}-b_{45}y_{2,1}^{0,1} \\ -b_{54}\nu_0 & -\nu_0^2 & b_{56}\nu_0 & b_{54}y_{1,1}^{0,1}+b_{56}y_{3,1}^{0,1}-2\nu_0 y_{2,1}^{0,1} \\ -b_{61} & -b_{65}\nu_0 & -b_{63}-\nu_0^2 & -2\nu_0 y_{3,1}^{0,1}-b_{65}y_{2,1}^{0,1} \end{pmatrix} \begin{pmatrix} y_{1,n}^{0,1} \\ y_{2,n}^{0,1} \\ y_{3,n}^{0,1} \\ \nu_{n-1} \end{pmatrix} = \begin{pmatrix} r_{1,n}^{0,1} \\ r_{2,n}^{0,1} \\ r_{3,n}^{0,1} \end{pmatrix}.$$

There is an unique value of ν_{n-1} such that this system is solvable. Then it remains a free parameter to determine $y_{1,n}^{0,1}$, $y_{2,n}^{0,1}$ and $y_{3,n}^{0,1}$. We set $y_{3,n}^{0,1}=0$, as mentioned in the discussion of the solution of the linear part, avoiding all ambiguities.

Finally we must compute the series of order n of y_4, y_5 and y_6. For this purpose we use (8). Note that for the computations we need y_1, y_2 and y_3 up to order n and y_4, y_5 and y_6 up to order $n-1$.

4 A SECOND ALGORITHM FOR THE LINDSTEDT–POINCARÉ PROCEDURE

We can proceed with the Lindstedt–Poincaré method working with the first order differential equations (4) instead of the second order ones. If we write down (8) explicitly, putting the linear part in the left hand side and the nonlinear one in the right hand one, we have

$$\begin{aligned} \dot y_1 - y_4 &= \sum q_{1i+3}g_{i+3}(Py), \\ \dot y_2 - y_5 &= \sum q_{2i+3}g_{i+3}(Py), \\ \dot y_3 - y_6 &= \sum q_{3i+3}g_{i+3}(Py), \\ \dot y_4 - b_{41}y_1 - b_{43}y_3 - b_{45}y_5 &= \sum q_{4i+3}g_{i+3}(Py), \\ \dot y_5 - b_{54}y_4 - b_{56}y_6 &= \sum q_{5i+3}g_{i+3}(Py), \\ \dot y_6 - b_{61}y_1 - b_{63}y_3 - b_{65}y_5 &= \sum q_{6i+3}g_{i+3}(Py), \end{aligned}$$

where $i=1,2,3$ in the summations. The series expansions for the functions y are the same ones as in the previous section. The derivatives which appear in the Lindstedt–Poincaré procedure are computed in the same way as before, but now only the first order derivatives appear.

Once the linear part is solved, at each step we must solve for the unknown part of order n. Proceeding in an analogous way as in the previous section we get the linear system of equations,

$$\begin{aligned} -\Psi y_{1n}^{km} - y_{4n}^{km} - \nu_{n-1}y_{11}^{01}\delta_{0k}\delta_{1m} &= r_{1n}^{km}, \\ \Psi y_{2n}^{km} - y_{5n}^{km} + \nu_{n-1}y_{21}^{01}\delta_{0k}\delta_{1m} &= r_{2n}^{km}, \\ -\Psi y_{3n}^{km} - y_{6n}^{km} - \nu_{n-1}y_{31}^{01}\delta_{0k}\delta_{1m} &= r_{3n}^{km}, \end{aligned}$$

$$
\begin{aligned}
\Psi y_{4n}^{km} - b_{41}y_{1n}^{km} - b_{43}y_{3n}^{km} - b_{45}y_{5n}^{km} + \nu_{n-1}y_{41}^{01}\delta_{0k}\delta_{1m} &= r_{4n}^{km}, \\
-\Psi y_{5n}^{km} - b_{54}y_{4n}^{km} - b_{56}y_{6n}^{km} - \nu_{n-1}y_{51}^{01}\delta_{0k}\delta_{1m} &= r_{5n}^{km}, \\
\Psi y_{6n}^{km} - b_{61}y_{1n}^{km} - b_{63}y_{3n}^{km} - b_{65}y_{5n}^{km} + \nu_{n-1}y_{61}^{01}\delta_{0k}\delta_{1m} &= r_{6n}^{km},
\end{aligned}
$$

where the series r represent the known part of the equation, $\Psi = k\omega + m\nu_0$, as before, and r_j is of the same type as y_j.

When $(k,m) \neq (0,1)$ we must solve,

$$
\begin{pmatrix}
-\Psi & 0 & 0 & -1 & 0 & 0 \\
0 & \Psi & 0 & 0 & -1 & 0 \\
0 & 0 & -\Psi & 0 & 0 & -1 \\
-b_{41} & 0 & -b_{43} & \Psi & -b_{45} & 0 \\
0 & 0 & 0 & -b_{54} & -\Psi & -b_{56} \\
-b_{61} & 0 & -b_{63} & 0 & -b_{65} & \Psi
\end{pmatrix}
\begin{pmatrix}
y_{1n}^{km} \\ y_{2n}^{km} \\ y_{3n}^{km} \\ y_{4n}^{km} \\ y_{5n}^{km} \\ y_{6n}^{km}
\end{pmatrix}
=
\begin{pmatrix}
r_{1n}^{km} \\ r_{2n}^{km} \\ r_{3n}^{km} \\ r_{4n}^{km} \\ r_{5n}^{km} \\ r_{6n}^{km}
\end{pmatrix}.
$$

The case $(k,m) = (0,0)$ gives a singular matrix, but since r_2, r_4 and r_6 are sinus type series, we have $r_{2n}^{00} = r_{4n}^{00} = r_{6n}^{00} = 0$ and so we can choose $y_{2n}^{00} = y_{4n}^{00} = y_{6n}^{00} = 0$ and to solve for the remaining equations.

Finally for the case $(k,m) = (0,1)$ (which only appears when n is odd) the previous matrix is again singular due to the determination of ν_0 during the computation of the part of order one. But then we solve,

$$
\begin{pmatrix}
-\nu_0 & 0 & 0 & -1 & 0 & 0 & -y_{11}^{01} \\
0 & \nu_0 & 0 & 0 & -1 & 0 & y_{21}^{01} \\
0 & 0 & -\nu_0 & 0 & 0 & -1 & -y_{31}^{01} \\
-b_{41} & 0 & -b_{43} & \nu_0 & -b_{45} & 0 & y_{41}^{01} \\
0 & 0 & 0 & -b_{54} & -\nu_0 & -b_{56} & -y_{51}^{01} \\
-b_{61} & 0 & -b_{63} & 0 & -b_{65} & \nu_0 & y_{61}^{01}
\end{pmatrix}
\begin{pmatrix}
y_{1n}^{01} \\ y_{2n}^{01} \\ y_{3n}^{01} \\ y_{4n}^{01} \\ y_{5n}^{01} \\ y_{6n}^{01} \\ \nu_{n-1}
\end{pmatrix}
=
\begin{pmatrix}
r_{1n}^{01} \\ r_{2n}^{01} \\ r_{3n}^{01} \\ r_{4n}^{01} \\ r_{5n}^{01} \\ r_{6n}^{01}
\end{pmatrix}
$$

for y_{1n}^{01}, y_{2n}^{01}, y_{3n}^{01}, y_{4n}^{01}, y_{5n}^{01}, y_{6n}^{01} and ν_{n-1}.

5 A SAMPLE OF THE ORBITS OBTAINED

Using the second algorithm of the previous section for the implementation of the Lindstedt–Poincaré procedure, we have done computations of quasihalo orbits in different situations: L_1 and L_2 equilibrium points in the Sun–Earth+Moon and Earth–Moon systems. We present in this section the results obtained for the L_1 point of the Sun–Earth+Moon system. The ones corresponding to the other equilibrium points or systems are qualitatively similar. All the computations have been done using order 25, both in the expansions in powers of γ and in the order of harmonics of the Fourier developments.

As a sample of the results obtained, figures 1, 2, 3 and 4 show the projections on the coordinate planes of some orbits. These orbits have been drawn using the results of the LP procedure. See later for the difference with respect to real orbits of the RTBP. All of them have been computed taking as backbone halo orbit one with z–amplitude $\beta = 0.2$. The value of the amplitude in km can be obtained multiplying this value by the unit of distance, which is taken equal to the distance from the equilibrium point to the nearest primary. In this case the primary is the Earth+Moon barycenter and the equilibrium point is L_1, so $\beta = 0.2 \times 1497610\text{km} \approx 300\,000\text{km}$. The four figures show quasihalo orbits with different γ amplitudes around this halo

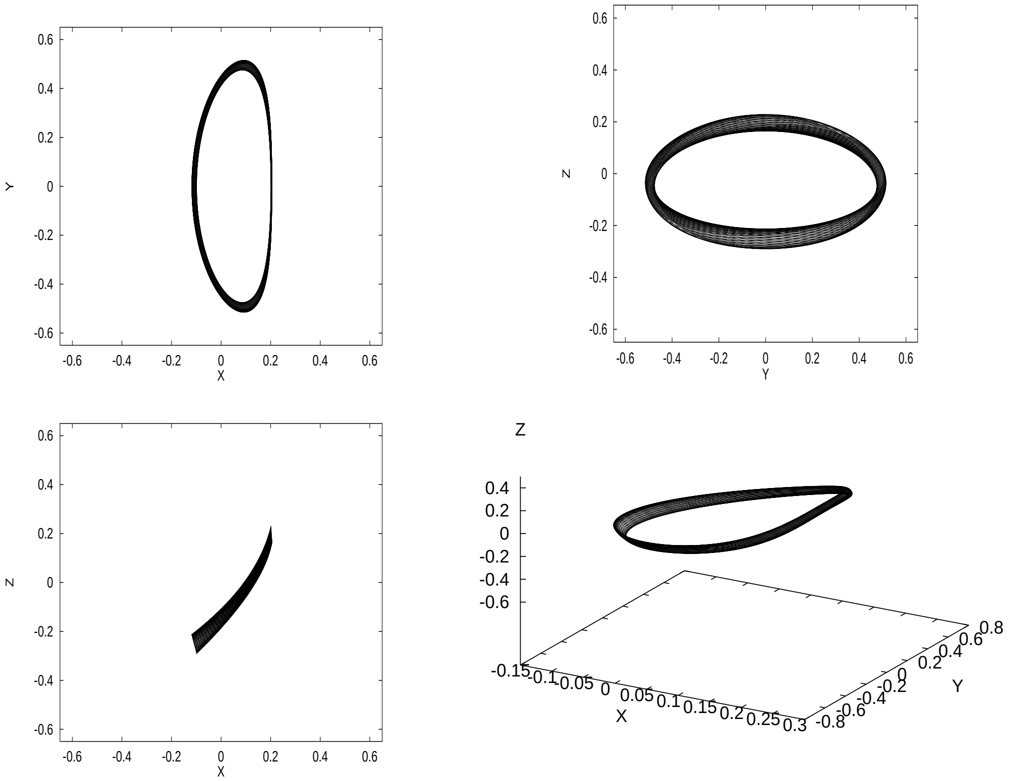

Figure 1: Projections on the coordinate planes and a 3D representation of the quasihalo orbit with $\beta = 0.2$ and $\gamma = 0.032$. For all the representations we have used the normalized reference system centered at the equilibrium point. In the 3D representation the aspect ratio is not 1:1:1.

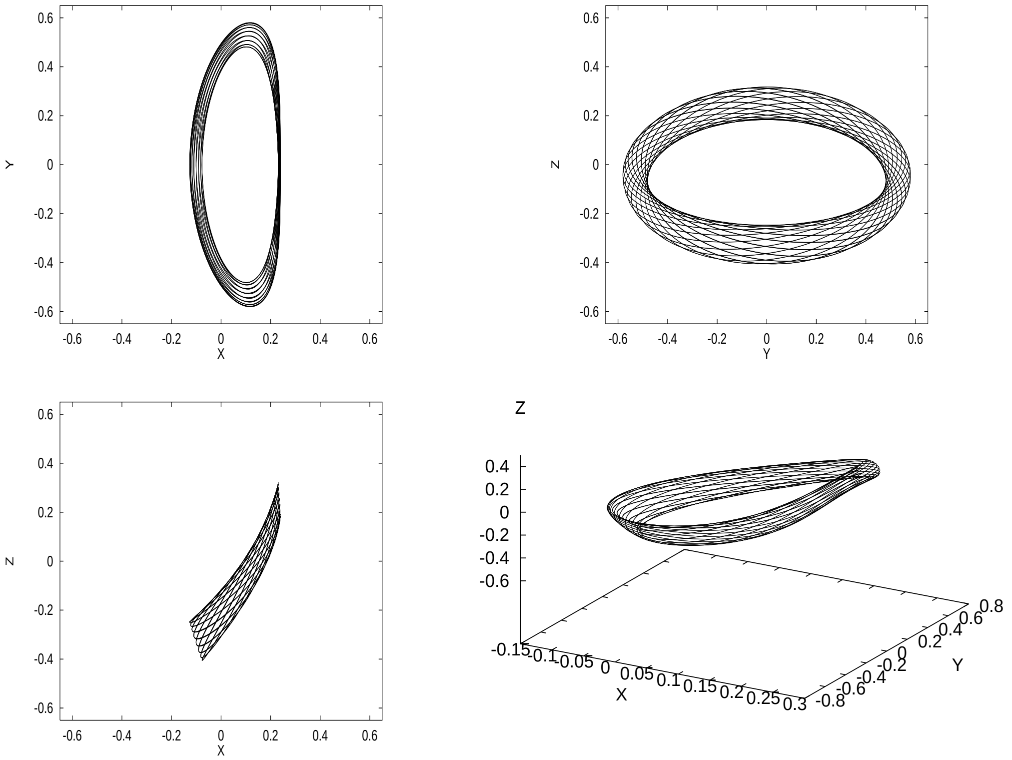

Figure 2: Projections on the coordinate planes and a 3D representation of the quasihalo orbit with $\beta = 0.2$ and $\gamma = 0.067$. For this value of γ we have almost resonance between the two basic frequencies and so the motion is very close to periodic.

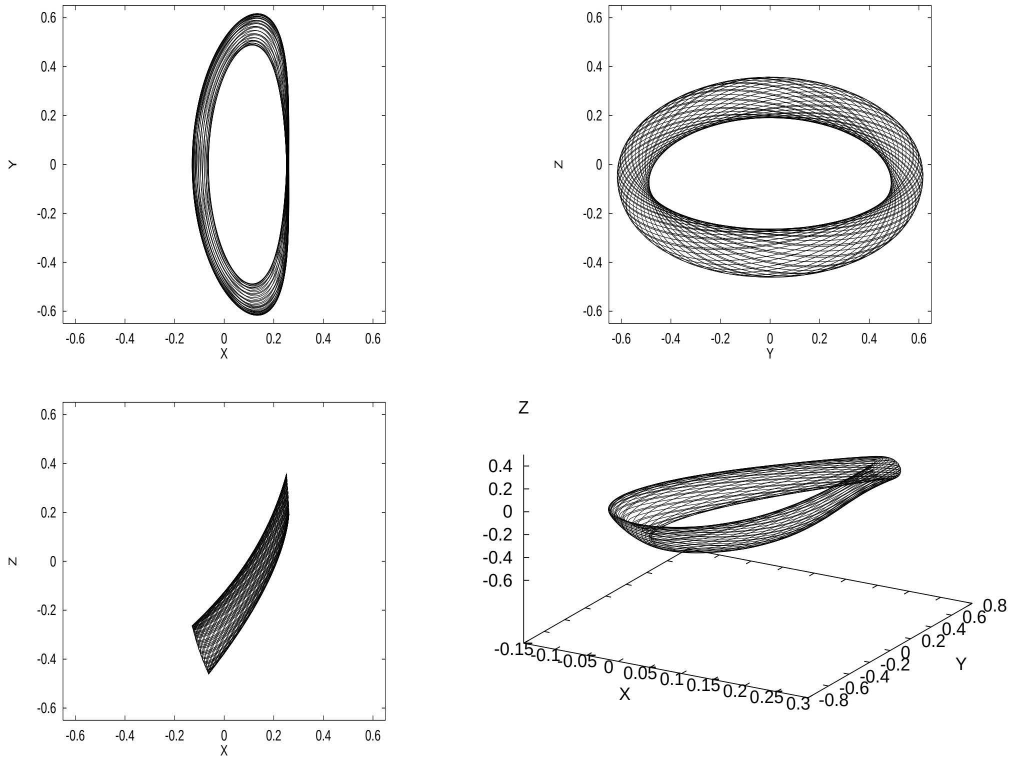

Figure 3: Projections on the coordinate planes and a 3D representation of the quasihalo orbit with $\beta = 0.2$ and $\gamma = 0.082$. This value of γ is close to the border of the region of practical convergence of the expansions.

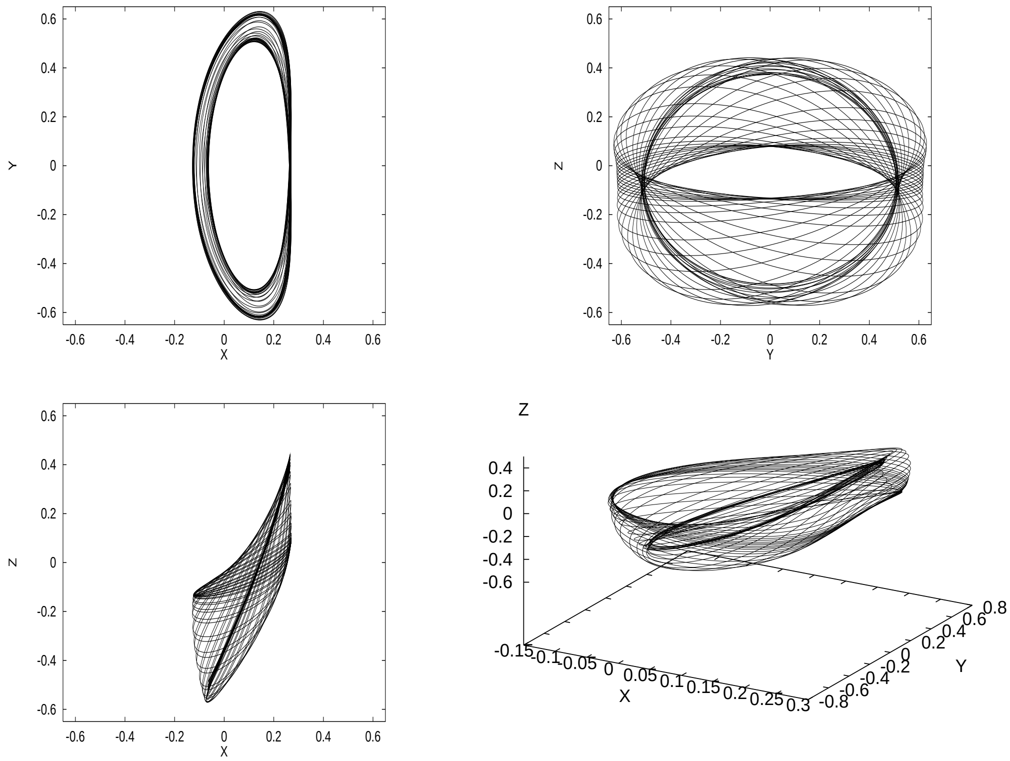

Figure 4: Similar to the previous figures for $\beta = 0.2$ and $\gamma = 0.090$. For this value of γ the expansions are out of the range of practical convergence.

orbit. The first one, in figure 1, has $\gamma = 0.032 \approx 48\,000$km and the motion is clearly quasiperiodic on a small torus around the halo orbit. Figure 2 corresponds to $\gamma = 0.067 \approx 100\,340$km. For this value of the amplitude, there is an almost resonance between the two basic frequencies of the motion, ω and ν, and so the motion on the torus seems to be periodic (ω=2.05584478..., and $\nu = 0.12105618..$, so $\omega/\nu = 16.98..$). Figure 3 is similar to figure 1, but with a larger value of γ which is very close to the border of the "practical region of convergence", as we will see later. Finally, figure 4 shows an orbit having some strange bendings. For this orbit, the value of γ is outside the practical region of convergence. All the orbits have been plotted for a time span corresponding to 40 revolutions of the basic halo orbit; this means 122 adimensional time units or, equivalently, 19.5 years.

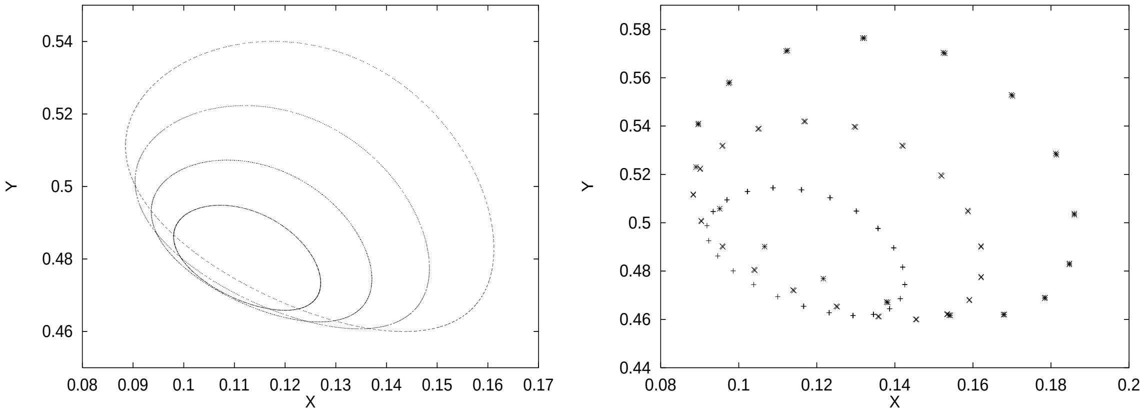

Figure 5: Intersections of the quasihalo orbits with $z = 0$, $\dot{z} > 0$. All the orbits have β=0.2. In the left figure the different "curves" correspond to γ =0.02 (inner curve), 0.03, 0.04, 0.05 (outer curve). In the right figure the values of γ (0.035 in the inner curve, 0.051 and 0.067 in the outer curve) are such that the motion on the tori is very close to periodic.

To have an idea of the thickness (that is, the size in a direction transversal to the backbone halo orbit) of the computed tori around the halo orbits, we have plotted their intersections with the surface of section $z = 0$, $\dot{z} > 0$, for different γ amplitudes. The results are shown in figure 5. In the left hand side figure, the points filling the different "curves" correspond to the quasihalo orbits with γ =0.02, 0.03, 0.04 and 0.05. All the motions look quasiperiodic and the orbits associated with each one of the curves fill up the corresponding torus. The points of the right hand side figure look like isolated points (at least if we represent a not very large number of intersections). For the amplitudes selected for this last figure, there is an (almost) resonance between the halo frequency and the normal to the halo frequency, which is close to 17:1 for the outer points (γ =0.067), 20:1 for the intermediate points (γ =0.051) and 23:1 for the inner points (γ =0.035). The pattern of these two figures is different from the standard one that is obtained when one computes iterates of the Poincaré map around a fixed point of a Hamiltonian system. In this latter case the "invariant curves" do not intersect each other as in our figures. This is due to the fact that in our case we have not kept fixed the value of the energy (Hamiltonian) for the different orbits displayed. We have done this for figure 6. In this figure, the value of the energy, given by the Hamiltonian of the RTBP in normalized units, and assigning the value zero to the L_1 point, is $h = 0.6$, which is the one corresponding to the periodic halo orbit with z–amplitude $\beta = 0.26097534$ (391 000 km approximately). This orbit should be represented as a fixed point of the Poincaré map located inside all the curves. The other curves correspond to quasihalo orbits of different values of γ that have been computed for different values of β too, in order to be on a fixed level of the energy. Notice that both frequencies for this level of energy change mildly with γ (see figure 7) for this range of γ, but certainly the ν frequency should go to zero when we approach the Lyapunov orbit at the boundary. For reference, a part of the planar Lyapunov orbit on the same level of energy is also shown (see also the discussion at the beginning of next section). This illustrates that "good" results are obtained, at least, up to one half of the distance to the planar Lyapunov orbit, for this energy. This means that up to this value of γ we are within the practical radius of convergence of the expansions. In the next section we will discuss the convergence of the series with more detail.

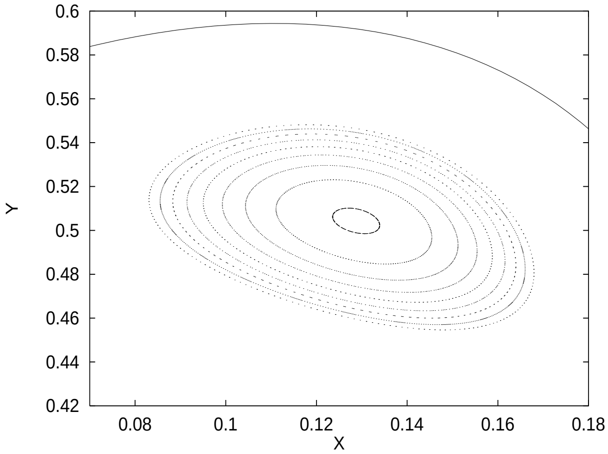

Figure 6: Intersection of the quasihalo orbits with $z = 0$. All the orbits have the same value of the Hamiltonian, $h = 0.6$. The different curves correspond (in the sense of decreasing sizes) to quasihalo orbits with $(\beta, \gamma) = (0.16, 0.0637702)$ (outer curve), (0.17, 0.0610280), (0.18, 0.0583477), (0.19, 0.0553808), (0.20, 0.0520384), (0.21, 0.0482263), (0.22, 0.0438212), (0.23, 0.0386083), (0.24, 0.0321922), (0.25, 0.0235894), (0.26, 0.0071181) (inner curve). For reference, also a part of the planar Lyapunov orbit on the same level of energy is shown (as continuous line).

In figure 7 we have represented the values of the two basic frequencies associated with the tori: the halo frequency, ω, and the frequency, ν. In the left figure we plot both frequencies (the halo one decreased by 2.05 units in order to reduce the size of the y–range and see more clearly how the frequencies vary) for different values of β. In this plot, for the frequency ν we have only taken the constant term, ν_0, of the series (11). That is, ν_0 is the normal frequency associated with the halo orbit. In the figure on the right, for different values of the normalized z–amplitude, β, between 0.05 and 0.25, the variations of the ν frequency with respect to γ are shown. The variations are rather small in all cases, associated with different base halo orbits, and the different lengths of the curves are related to the different practical convergence radii that we have when β varies, as we will see in the next section.

Concerning the instability properties of the quasihalo orbits, they are essentially the same as those of the base halo orbits: when β increases, the orbits become less unstable, but in all cases they display a strong instability. This fact becomes clear when we compute the maximal Lyapunov number associated with these orbits. As the time t increases, the maximal Lyapunov number stabilizes in a fast way around a positive value. In figure 8 we show a typical behaviour for the case of a quasihalo orbit with $\beta = 0.15$ and $\gamma = 0.02$ of the S–E+M around the L_1 point for the first 1000 days. In this case it tends in a rather fast way to a value close to 2.415. This value is always very close to the Lyapunov number associated with the periodic halo orbit. Notice that despite previous plots were done for 122 adimensional time units, this time span is too small to get a good enough determination of the maximal Lyapunov number. In figure 8 a value of 1000 units has been used. This is possible because the analytic approximation of the orbit is known. In spite of this instability, the spacecraft can be controlled in practice by rather cheap station-keeping strategies. The related geometric ideas and the technical details can be found, for the case of halo orbits, in [11], [12], [3], [22] and [20]. The modifications to deal with the quasihalo orbits are easy.

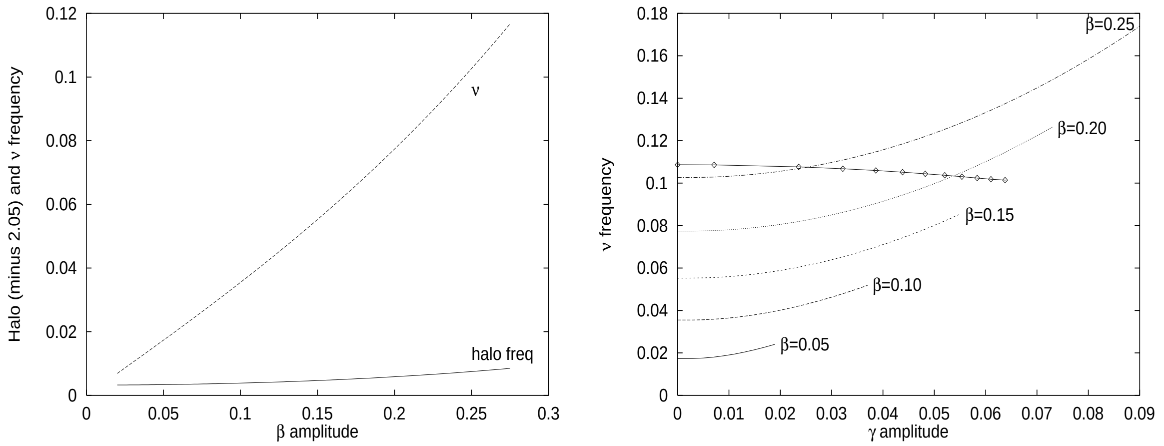

Figure 7: In the left figure we plot, for different β amplitudes, the frequency of the halo orbit (minus 2.05) and the normal frequency ν_0. On the right figure, for different values of β (0.05, 0.10, 1.05, 0.20 and 0.25), the corresponding ν frequency of the quasihalo orbit, when the γ amplitude varies, is represented. For completeness the right figure also shows the values of the ν frequency of the orbits, on $h = 0.6$, displayed in figure 6. The corresponding values of the ω frequency can be read from the left figure, depending only on β .

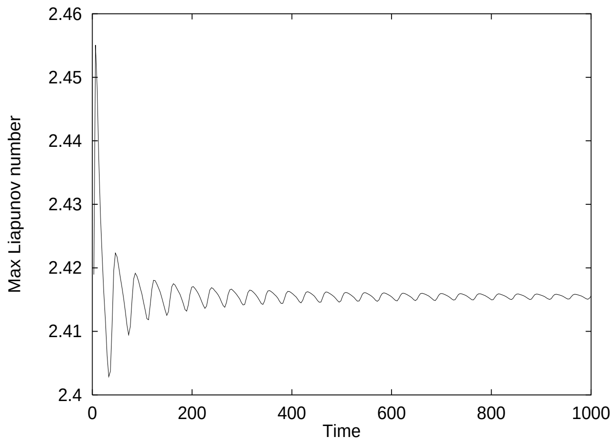

Figure 8: Evolution of the approximation to the maximal Lyapunov number versus time (in adimensional units) for a quasihalo orbit with $\beta = 0.15$ and $\gamma = 0.02$ of the S–E+M around the L_1 point.

6 CONVERGENCE OF THE SERIES

A global study of the orbits in a large neighbourhood of the collinear equilibrium points is done in [12]. Figure 9 (from [24]) displays a representation of the globality of the orbits in the L_2 E–M case for $h = 1$. See [12] for similar results for the L_1 point of the S–E+M case and other values of the energy. This figure shows the dynamics in a Poincaré section of the flow reduced to the center manifold, $W^c_{L_2}$ (see also [37] for details on the reduction to $W^c_{L_2}$). It has been done using some suitable coordinates, but the section displayed is very close (even quantitatively) to a section through $z = 0$, skipping all the influence of the instability. Note that, for aesthetic reasons, the figure is rotated by 90 degrees. So, the normalized positive x axis points upwards and the positive y axis goes to the left, the Moon being located at unit distance on the negative

x axis. The boundary curve of the Poincaré section corresponds to the planar Lyapunov orbit. As this orbit is on $z = 0$, the flow is no longer transversal to the section along it. This orbit is unstable even on $W^c_{L_2}$. Halo orbits are born at the level of energy such that the planar Lyapunov orbit changes from stable to unstable inside $W^c_{L_2}$. The central fixed point corresponds to the vertical Lyapunov orbit, while the other two fixed points correspond to the class I and II halo orbits. Around each one of the fixed points there are open regions almost foliated by invariant curves, which represent the Lissajous orbits close to L_2 and the present quasihalo orbits around the halo ones. Both types of curves correspond to 2D tori in the full phase space. The boundary between these regions are stochastic zones (very narrow even for the relatively big energy level displayed) associated with the part of the stable/unstable manifolds of the planar Lyapunov orbit that remains on $W^c_{L_2}$. From this it follows that, for a fixed value of the Hamiltonian, there is a maximum value for the amplitude γ (distance to the halo orbit) beyond which we do not have quasihalo orbits. The "bound" for the amplitude γ is the stochastic region associated with the manifolds of the planar Lyapunov orbits and the proper planar Lyapunov orbits. In fact, the size of the region, around the fixed point (representing the halo orbit) where the quasihalo orbits are found, varies with the energy or, equivalently, with the amplitude of the backbone halo orbit. Compare (qualitatively) the curves in figure 9 around the halo orbit on the right (and a part of the planar Lyapunov orbit) with the ones in figure 6 (after rotating the latter one by -90 degrees).

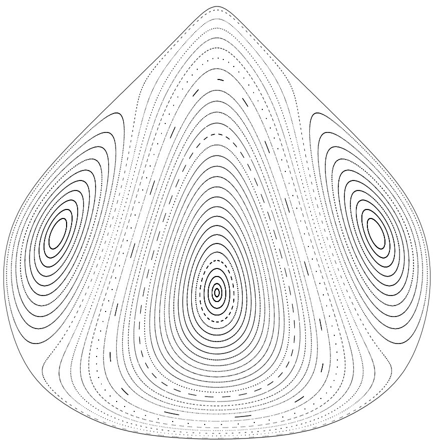

Figure 9: Poincaré section of the center manifold associated with the collinear point L_2 of the E-M system, for a value of the normalized Hamiltonian $h = 1$.

On the other hand, the series that we have produced for these orbits are asymptotic but divergent everywhere. This is due to the fact that there does not exist any open set foliated by 2D tori. Nevertheless, the resonances, which produce small stochastic zones associated with the divergence, show up only when the expansion is carried up to at least the order of the resonances. So, their "influence", for moderate time intervals, is rather small and, in principle, difficult to detect. As an illustration, for the case shown in figure 9, which corresponds to a high value of h, the rotation number on the invariant curves around the central fixed point decreases from $\simeq 1/12.4157$ to some value close to 0, while for the invariant curves around the halo orbits it decreases from $\simeq 1/8.5578$ to something close to zero. Hence, the lowest order resonance is the 1:9 one. Furthermore, standard KAM arguments can be used to prove rigorously the existence of these Lissajous type orbits (see [25], [26], [27]) in the RTBP and in quasiperiodic perturbations of it, if the size of the perturbation is small enough.

We have computed "practical" radii of convergence of the power series in γ of the quasiperiodic halo orbits obtained, using different criteria. As it has been said, these radii vary with the

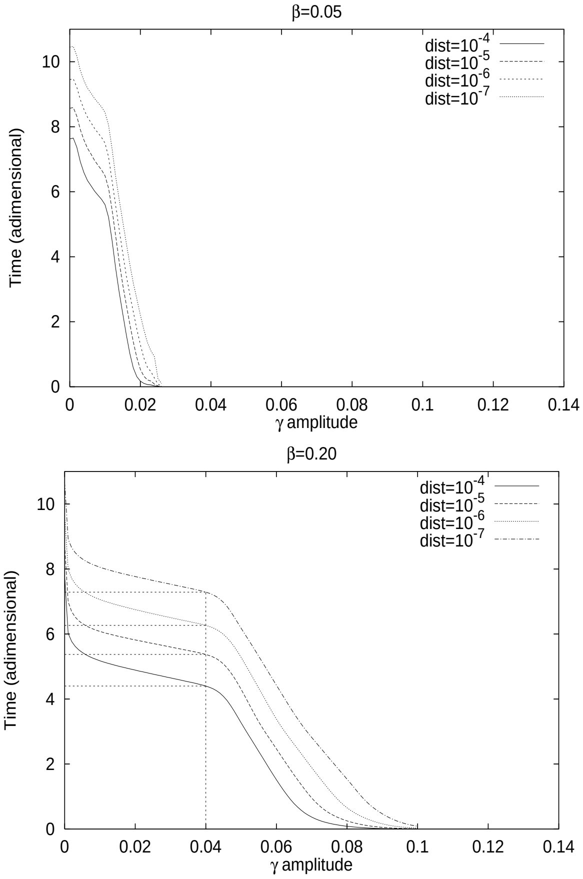

Figure 10: Escape time vs γ for different distances. Case of L_1 for the S–E+M problem. The different curves displayed in each one of the figures show the escape time versus γ when varying the distance adopted as the escape distance. The values taken are 10^{-n} , $n = 4, 5, 6, 7$ in adimensional units (physically 15 000, 1 500, 150 and 15 km, in distances). All the computations have been done using order 25 for the expansions. The different figures correspond to different values of β: 0.05, 0.10, 0.20 and 0.25. For $\beta =$ 0.20 we have displayed the epochs of escape at the different distances, which are 4.400, 5.371, 6.266 and 7.289 adimensional time units.

amplitude β of the reference halo orbit. We will give the results for the L_1 and L_2 equilibrium points in both the Sun–Earth+Moon and Earth–Moon systems.

Before going into the discussion of the different methods used for the determination of the radius of convergence, we present some previous checks of the goodness of the computed solutions. We can compare the solutions obtained with the LP procedure with those computed by numerical integration of the differential equations of the RTBP taking, of course, the same initial conditions. We fix a certain maximum separation in the configuration space, and we stop the integration when this separation is reached. We have done the comparison using the expansions for the quasihalo orbits up to order 25.

In figure 10 the results for the Sun–Earth+Moon system L_1 point are shown taking as maximum separation the values 10^{-4}, 10^{-5}, 10^{-6} and 10^{-7} in adimensional units (physically this corresponds, in distance, to 15 000, 1 500, 150 and 15 km, respectively). In this figure the computations have been done for different values of the amplitude of the base halo orbit, and varying, for each one, γ. Of course, in all cases one should have escape because of the strong intrinsic instability of these orbits. For a fixed value of β, let γ move in the decreasing sense. If we are in the non "convergence" region the escape is very fast. When the boundary of the "convergence" zone is reached, the orbits remain nearby for a time interval that varies between 4 and 9 adimensional time units (2π adimensional units = 1 year). This variation depends mainly on the maximum separation allowed, and very mildly on the size of the base halo orbit, given by its z–amplitude β. After this time interval, the escape is very fast due to the strong unstable character of the solutions considered. The explorations have been done for a large set of initial conditions obtained by varying the initial phases of the quasihalo orbit at the initial epoch. All the results are close to the ones presented here which correspond to both phases equal to zero. For the Earth–Moon system and the other equilibrium points, the results are qualitatively very close. These curves also allow us to estimate the error in the initial conditions (see figure 11). For instance, for $\beta = 0.2$, $\gamma = 0.04$ and an adimensional distance of 10^{-7}, the "good agreement adimensional time" is roughly 4.4. Using a maximal Lyapunov exponent of 2.39 the intrinsic effect of the instability can increase the errors by $\exp(4.4 \times 2.39) \approx 3.7 \cdot 10^4$. This means that the initial errors are of the order of $2.7 \cdot 10^{-12}$ in adimensional units, i.e., 40 cm in physical units in the S–E+M case and 1 mm in the E-M case. The comparison of the different curves also allows us to estimate the maximal Lyapunov exponent. Again for $\beta = 0.2$ and $\gamma = 0.04$, an increase of the distance by a factor of 10 requires, on the average, $(7.289–4.400)/3 = 0.963$ units of adimensional time (see the suitable data on the caption of figure 10). This gives a maximal Lyapunov exponent of $\ln 10/0.963 \approx 2.39$. Using this, an estimate of the error (in the unstable direction) at $t = 0$ is given for the values of β and γ of figure 10 in figure 11 as well as an estimate of the maximal Lyapunov exponent in figure 12.

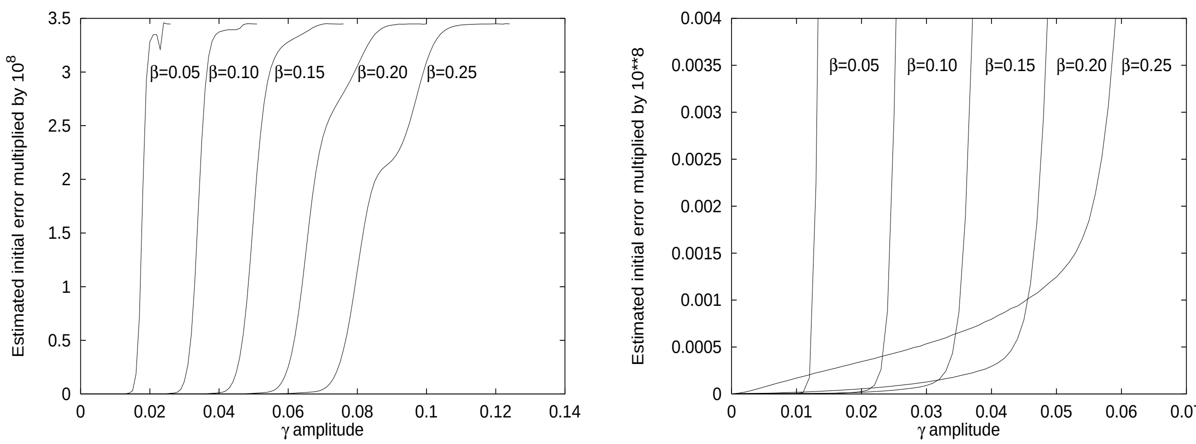

Figure 11: On the left figure we show, at $t = 0$, the error in the unstable direction vs γ, for different values of β. On the right figure a magnification of the lower left corner is shown. From these figures is clear that the error of the expansion of the quasihalo orbits is very small when we are close to the backbone halo orbit. This error increases very fast when a certain value of γ is reached. This value of γ varies with the β amplitude of the backbone halo orbit and agrees with the values at which the slope changes in the curves of figure 10.

A first rough estimate of the convergence radius of the series can be done in the following way. For a fixed value of β we can compute the frequency ν truncating its series (11) at different orders. This is shown in figure 13 for β=0.20 in the S–E+M system for the L_1 case. The values obtained with different truncations are in good agreement up to values of γ approximately equal to 0.08. This value can be taken as a first empirical approximation for the practical convergence radius. For this figure the expansions have been computed and used up to order 35.

If we apply the quotient or the root criterion to the series (11), it is seen that the values obtained for the radius of convergence at the different orders, in general, tend in a fast way to a stabilizing one. This is true if the value of the β amplitude of the halo orbit is such that there is no resonance between the halo frequency, ω, and the normal frequency, ν_0, or if the order of the resonance is high (i.e. greater than 20). In figure 14 we show the values obtained for the radii,

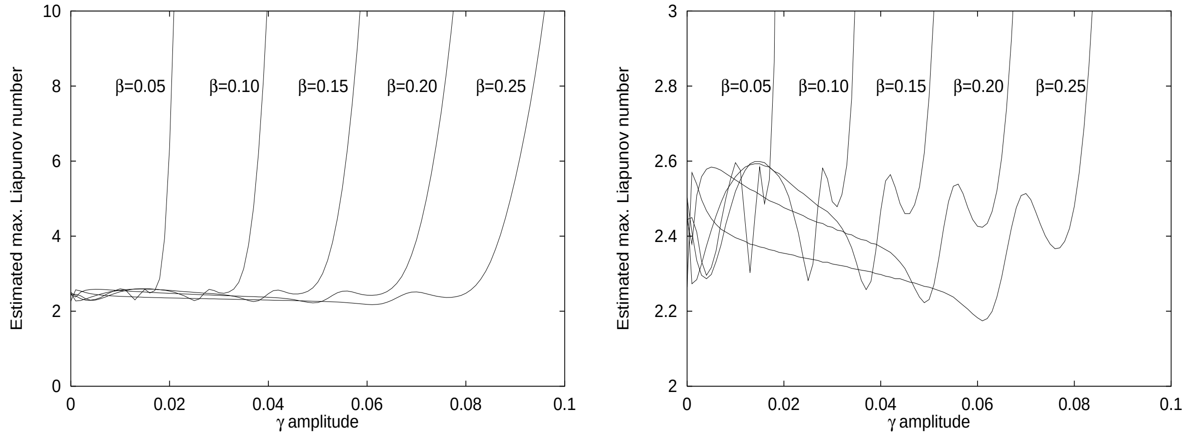

Figure 12: On the left figure estimated maximal Lyapunov number vs γ amplitude for quasihalo orbits around halo orbits with β=0.05, 0.10, 0.15, 0.20 and 0.25. On the right figure a magnification of a suitable window in the vertical direction is displayed. The figure has been obtained with the data used to get figure 10 and some additional data for $\beta = 0.15$.

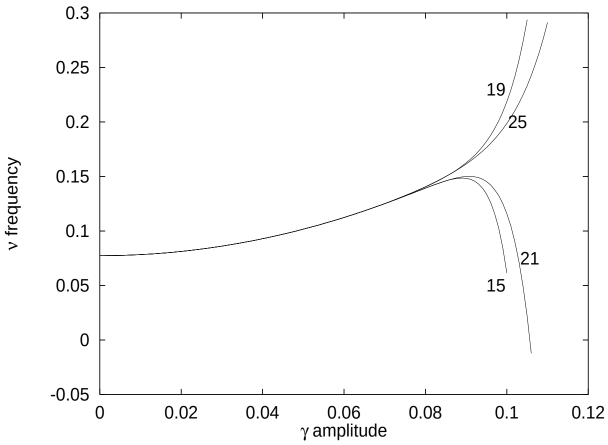

Figure 13: For a basic halo orbit around L_1 in the Sun–Earth+Moon system with $\beta = 0.20$, values of the ν frequency when varying γ. ν has been computed using six different maximum orders for its expansion (25, 27, 29, 31, 33 and 35). The differences become significant for values of γ greater than 0.08, approximately, which agrees with other estimates of the radius of convergence.

using both estimates, as a function of the order of the expansion and for two values of the β amplitude in the S–E+M case, L_1 point. The first value of β is 0.2 for which the values of both frequencies are $\omega = 2.0558447898$, $\nu_0 = 0.0773857270$ and its quotient is approximately 26.5662. In the right hand side figure the value of β is 0.402 (a nearby value appears in table 1, see later), the values of the frequencies are $\omega = 2.0664193648$, $\nu_0 = 0.2069134669$ and now its quotient is 9.9868, which is very close to the $1 : 10$ resonance. In the first figure both criteria give qualitatively similar results and a value for the convergence radius around 0.08. In the second case the values of the convergence radius given by both criteria clearly go to zero. In fact, with the quotient criterion the value is "almost" zero when the order of the serie is larger than 27. Of course, increasing the order of the expansions, will lead to divergence. Using the quotient criteria, once the estimates of the radius are close to a stabilized value (which usually happens when the order is greater than 15), we have taken the maximum and minimum values of the quotients as upper and Lower estimates of the radii of convergence. These are the values that are represented in figure 15 for different values of β, also in the S–E+M system for the L_1 case.

For β=0.2, the value of the lower estimated radius is 0.084 which is close to all the estimates obtained before.

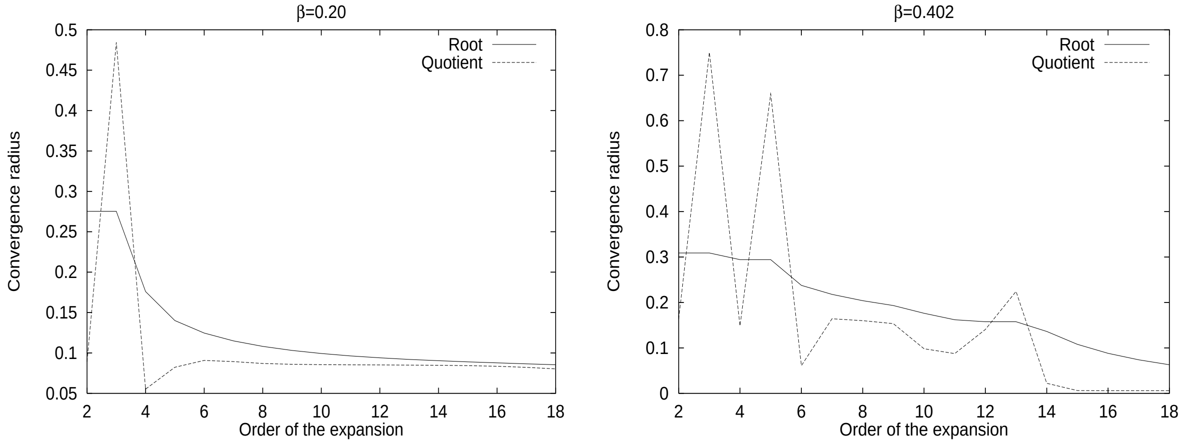

Figure 14: Behaviour of the "convergence" radii of the series (11) vs the order of the expansion. The estimates have been computed using the quotient and the root criteria and the series has been computed up to order 35. Both figures correspond to quasihalo orbits of the S–E+M system, L_1 point. The left figure is for a value of the amplitude $\beta = 0.2$ and the right figure for $\beta = 0.402$, which is close to the 1:10 resonance (see explanations in the text).

When, for a fixed value of β, γ varies between zero and the most pessimistic estimate for the radius of convergence, we can compute the energy of the different orbits given by the value of the Hamiltonian. In this way, we can represent a domain of "practical convergence" in the (β-h) plane, where h is the value of the Hamiltonian. The shaded area of the right hand side picture of figure 15 shows this region. In this figure, cutting the dotted region with the horizontal line h=0.6, we determine the range of values of the β amplitude for the orbits that are plotted in figure 6.

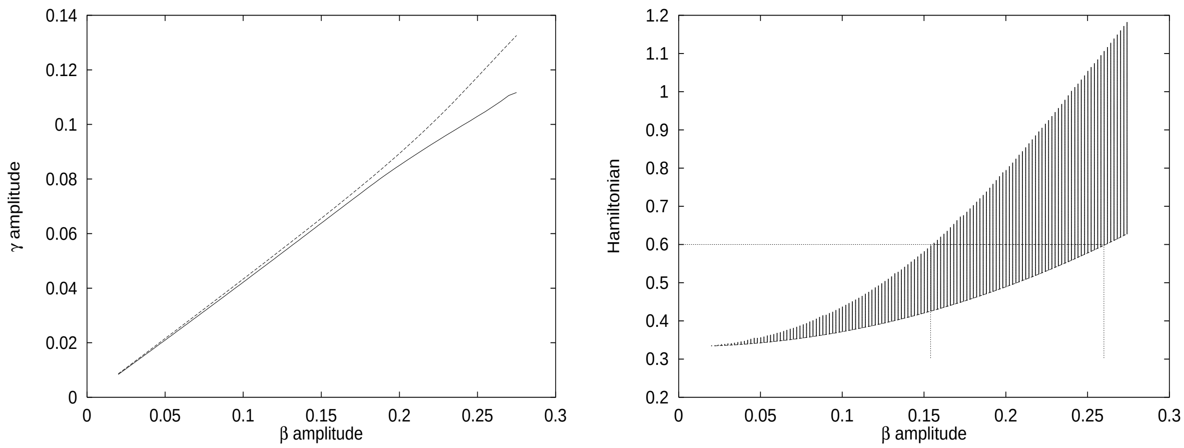

Figure 15: In the left figure the two curves are the γ values of the upper and lower estimates for the practical radius of convergence of ν, for different values of β. In the right figure the dotted region corresponds to the convergence domain in terms of the value of the Hamiltonian. In this figure the lower boundary of the shaded area corresponds to the halo orbits ($\gamma = 0$) and, for a fixed value of β, γ varies between 0 and the lower curve of the left figure. All the computations correspond to the Sun–Earth+Moon system and the L_1 point.

The other two determinations that have been done use the expansions of the coordinates

(10). The first one is close to the check presented at the beginning of this section and compares the formal series solution and the solution obtained by numerical integration of the RTBP equations. At the initial epoch, $t = 0$, we set as initial conditions for the numerical integration the ones given by the expansions. We perform the integration for π adimensional time units (which

Sun–Earth+Moon, L_1				Sun–Earth+Moon, L_2			
β	ω	ν	ω/ν	β	ω	ν	ω/ν
0.29504115	2.05940821	0.12871301	16	0.27117583	2.03166338	0.11287019	18
0.30871720	2.06009519	0.13733968	15	0.28278049	2.03230169	0.11954716	17
0.32369948	2.06090849	0.14720775	14	0.29538756	2.03304024	0.12706502	16
0.34019524	2.06188334	0.15860641	13	0.30913715	2.03390229	0.13559349	15
0.35846121	2.06306900	0.17192242	12	0.32419849	2.03491867	0.14535133	14
0.37881966	2.06453646	0.18768514	11	0.34077823	2.03613116	0.15662548	13
0.40168114	2.06639170	0.20663917	10	0.35913178	2.03759774	0.16979981	12
				0.37957909	2.03940126	0.18540012	11
				0.40252649	2.04166424	0.20416642	10
				0.42849765	2.04457555	0.22717506	9
				0.45817641	2.04844182	0.25605523	8
Earth–Moon, L_1				Earth–Moon, L_2			
β	ω	ν	ω/ν	β	ω	ν	ω/ν
0.29141854	2.27846077	0.14240380	16	0.26164515	1.85214701	0.09748142	19
0.30448524	2.27741589	0.15182773	15	0.27274805	1.85332147	0.10296230	18
0.31881602	2.27623386	0.16258813	14	0.28477565	1.85466738	0.10909808	17
0.33462253	2.27488999	0.17499154	13	0.29784677	1.85622054	0.11601378	16
0.35217053	2.27335431	0.18944619	12	0.31210204	1.85802702	0.12386846	15
0.37179911	2.27159070	0.20650825	11	0.32770936	1.86014711	0.13286765	14
0.39394864	2.26955663	0.22695567	10	0.34487088	1.86266120	0.14328163	13
				0.36383243	1.86567896	0.15547324	12
				0.38489594	1.86935392	0.16994126	11

Table 1: Resonant β values, halo and normal frequencies and order of the resonance.

means half a year for the S–E+M system and half a synodic lunar month for the E–M system). After this time we compare the final point with the one obtained with the asymptotic expansions at the same epoch. If the distance between both, in the configuration space, is smaller than a given amount (that we have fixed to 10^{-6} adimensional units in both systems) we say that we have "convergence" for the parameters β and γ defining the quasihalo orbit. Using a maximal Lyapunov number of, say, 2.4, this corresponds to an initial error of the order of $10^{-6}\exp(-2.4\cdot\pi) \approx 5.3\cdot 10^{-10}$, i.e. approximately 0.08 Km in the S–E+M case and 0.2 m in the E-M one. However, there are two more free parameters that can vary: the two phases ϕ_1 and ϕ_2 that appear through the angles Φ_1 and Φ_2 of the equations (10). The convergence criterion takes care of them and, in fact, we say that we have convergence for given values of β and γ, if for a regular grid of 64 different values in $[0, 2\pi]\times[0, 2\pi]$ of the two phases, the minimum separation condition is fulfilled for all the phases. The results of this exploration are shown in figure 16. If the value of the threshold, 10^{-6}, is changed, the figures are qualitatively close to the ones represented, and they are over or below the displayed curves according if we increase or decrease the value of the threshold, respectively. The maximum value of β that is reached in the four situations, which is of the order of 0.40 units, is related to the maximum size of the basic halo orbit for which the corresponding analytical expansions look convergent. As it is seen, there is, for all the situations, a value of β for which a maximum value of γ is reached. This value of β is close to 0.27 except for the E–M system around the L_2 point. One of the most interesting features of the displayed curves is the presence of "sharp downwards peaks" at the right hand side of the maximum. Going through them the γ amplitude decreases in a very sharp way, as if the radii of convergence should be zero for some values of β. As we shall see, these peaks also appear, between the same values of β, when other convergence criteria are used. This is reminiscent of the instability tongues appearing in several problems (Mathieu equation, Arnold tongues, etc. See, for instance, [5], [4] and references therein).

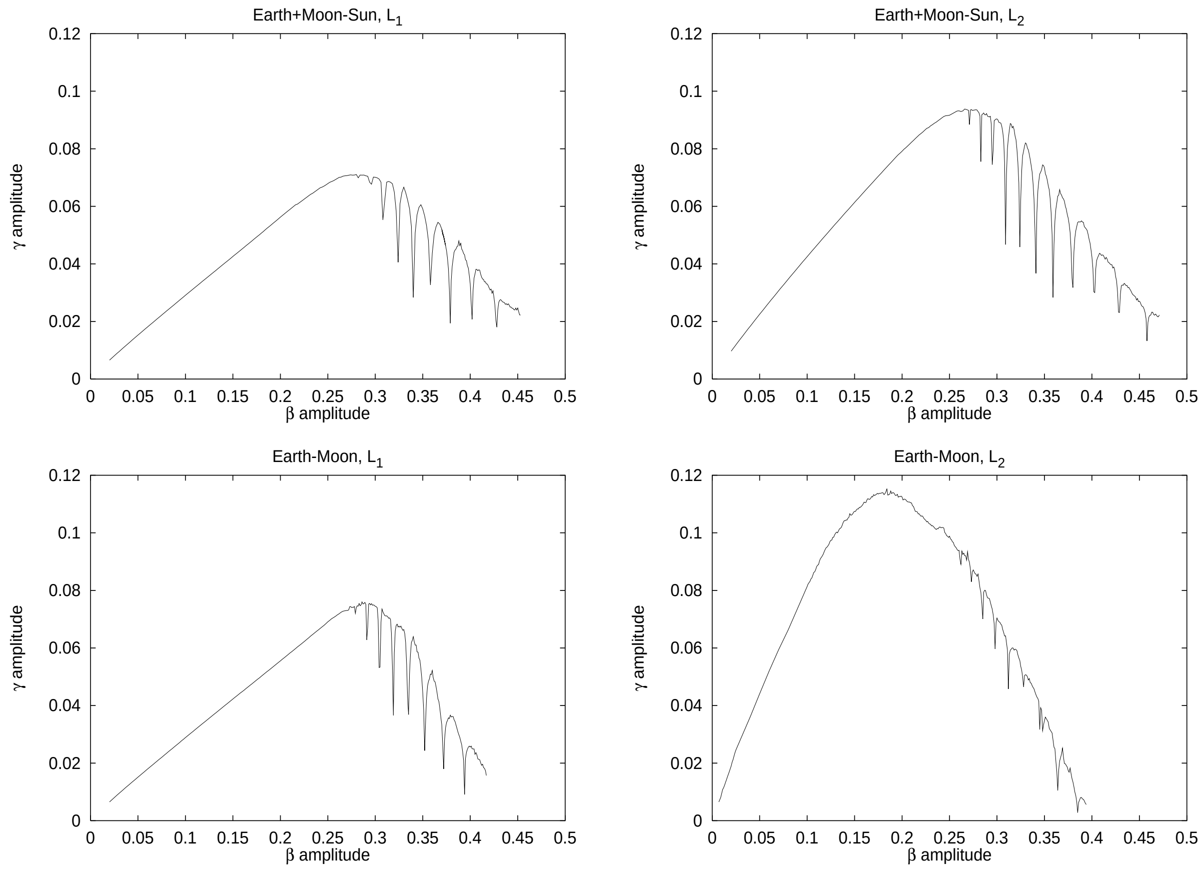

Figure 16: First estimate of the practical radius of convergence of the expansions for the coordinates. The computations have been done by integrating the RTBP equations of motion during π time units. For a fixed value of β the initial conditions to start the integration are computed using (10) for increasing values of γ, starting at $\gamma = 0$ and different values for the phases, for each value of γ. If after π time units the distance in the configuration space, between the point computed by numerical integration and the one computed using the expansions is smaller than 10^{-6} adimensional units (for all the values of the grid of 64 phases explored), the value of gamma is increased, else a new value of β is explored. For each β, the maximum value of γ reached is the one displayed in the figures. The upper figures correspond to the Sun–Earth+Moon system and the lower ones to the Earth–Moon system. The left figures correspond to the L_1 case and the right ones to the L_2 case. These figures can be produced from plots like the ones displayed in figure 10 by taking the 10^{-6} curve and cutting through time $= \pi$. They produce more severe results than the ones shown in figure 15.

The second procedure used for the determination of the practical radius of convergence is based in the computation of the residual accelerations. If we use the first algorithm of the LP

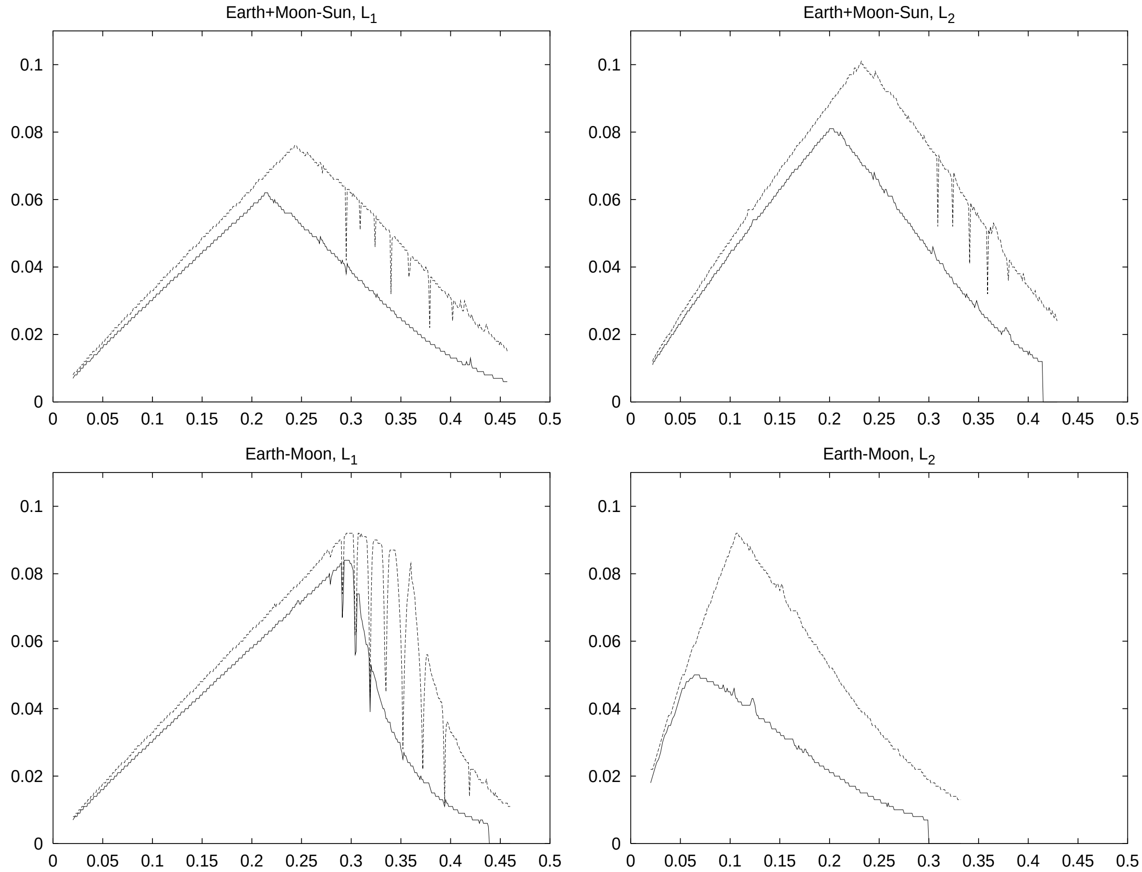

Figure 17: Second estimate of the practical radius of convergence of the expansions for the coordinates. The computations have been done computing the residual accelerations. These are defined in the following way. For a given set of amplitudes and phases, defining a quasihalo orbit, we fix an epoch. At this epoch we can compute, using the expansions for the coordinates, the position, velocity and acceleration of the spacecraft. We can also substitute the position and velocity obtained with the expansions in the right hand side of the equations of the RTBP, in this way we get a second value of the acceleration. Both values of the accelerations will be different due to the truncations of the expansions. The difference between both defines an error vector whose modulus is the residual acceleration. We have fixed a threshold for the maximum value allowed for the residual acceleration. For a fixed value of β we vary γ, and we compute the corresponding residual accelerations for different values of the phase ϕ_2 and time (ϕ_1 has been taken equal to zero and the different epochs that have been chosen correspond to taking a large number of points, 400, equally spaced in time, on a given number of revolutions around the equilibrium point, approximately 200). If all the points associated to a fixed value of β and γ have a residual acceleration less than the fixed threshold, the value of γ is increased, else we change the value of β. The two curves represented in the different plots correspond to two different values of the threshold: 10^{-6} (upper curve) and 10^{-7} (lower curve) in adimensional units. The upper figures correspond to the S–E+M system and the lower ones to the E-M system. The left figures correspond to the L_1 case and the right ones to the L_2 case.

procedure, we get the expansion of the position coordinates, and if we use the second algorithm we get positions and velocities. In both cases it is easy to get, by differentiation, the expansions of the accelerations. Once we have in hand the formal series for all the coordinates, we can evaluate them by setting the values of the parameters that remain free: γ, ϕ_1 and ϕ_2 and time. In fact these parameters are not independent. One can fix one phase (setting $\phi_1 = 0$, for instance) and vary ϕ_2 and time or fix time and vary the two phases. In the computations we have fixed the first phase to the value zero. (The value of β must be fixed before starting the full procedure. It is possible to compute the formal solutions as a double series in β and γ, and this was our first approach to the problem, but the resulting series have a very small domain of practical convergence, which makes them useless.) For a fixed set of values of the free parameters, we get a value for the acceleration. The acceleration associated with a given position and velocity can also be computed replacing the values of the position and velocity in the right hand side of the equations of the RTBP. The difference between the two accelerations is denoted as the *residual acceleration*. If the expansions were convergent, the residual acceleration would be zero when using the full series expansions, but as we have truncated them at some order and, furthermore, they are not convergent and only asymptotic, this will not happen. We have computed the residual accelerations for a large set of parameters. If for fixed values of β and γ and for all the values of the phase ϕ_2 and time explored, the residual acceleration is less than a given amount, we say that we have convergence. We used 8 uniformly distributed values in $[0, 2\pi]$ of ϕ_2 and 400 suitable values of time to have a good equidistribution on the corresponding torus. The results are shown in figure 17 taking two different values for the maximum value allowed for the norm of the residual acceleration. From a qualitative point of view the results are close to the ones obtained with the previous procedure. The value of the radius γ increases almost linearly with β until a maximum value is reached. Both the slope of the line and the value of the maximum agree with the previous computations. From the value where the maximum is achieved to the right, the behaviour is not so clean. There also appear the downwards peaks that we found when comparing only positions after π units of time. The values of β corresponding to the minima are also the same ones. These peaks are related to low order resonances between the two frequencies, ω and ν, that make zero the argument Ψ that appears in equation (13). As β increases, the order of the resonance decreases one unit at each singular value of β. We have refined the values of β to get the resonant values with more precision (the variations with respect to the values displayed in figures 16 and 17 are less than 0.001). The results are given in table 1, where we give, for each refined value of β, the halo, ω, and the normal, ν, frequencies as well as its quotient.

7 NUMERICAL REFINEMENT BY MULTIPLE SHOOTING

The purpose of this section is to get solutions of more realistic equations of motion (i.e., Newton's equations using some JPL model for the motion of the bodies of the solar system) that remain close to the solutions obtained for the RTBP in the previous sections. As a first restriction, considering that we are going to compute these solutions numerically, we will fix a time span, which means we will fix an initial epoch (now the system is non autonomous) and a length for the time span.

The general idea is to use a multiple shooting method similar to the one used for the numerical solution of boundary-value problems (see [38]). This method is useful for the computation of highly unstable periodic orbits with very long periods. Our problem is, in some sense, close to this one. As in the standard procedure, first we split the total time span into a number of shorter subintervals selecting, for instance, N equally spaced points $t_1, t_2, ..., t_N$. (t_1 is the initial epoch and $t_N - t_1$ the length of the time interval mentioned above). Different time intervals can be used, but we have chosen here all of them equal. Denote by $\Delta t = t_{i+1} - t_i$ and by

$$Q_i = (t_i, x_i, y_i, z_i, \dot{x}_i, \dot{y}_i, \dot{z}_i,)^T, \quad i = 1, 2, ..., N$$

the points on a fixed quasihalo orbit of the RTBP, equally spaced (Δt) in time, computed using the formal expansions. Let $\phi(Q_i)$ be the image of the point Q_i under the flow associated to the equations of motion in the solar system after an amount of time Δt. As, in this way, the epochs t_i are fixed, we can write $Q_i = (x_i, y_i, z_i, \dot{x}_i, \dot{y}_i, \dot{z}_i,)^T$. If all the points Q_i would be on the same orbit of the new equations, then $\phi(Q_i) = Q_{i+1}$ for $i = 1, ..., N-1$. As this is not the case, we need to change the starting values to fulfill the matching conditions. In this way, we must solve a set of $N-1$ nonlinear equations, which can be written as

$$F\begin{pmatrix} Q_1 \\ Q_2 \\ \vdots \\ Q_N \end{pmatrix} = \begin{pmatrix} \phi(Q_1) \\ \phi(Q_2) \\ \vdots \\ \phi(Q_{N-1}) \end{pmatrix} - \begin{pmatrix} Q_2 \\ Q_3 \\ \vdots \\ Q_N \end{pmatrix} = \Phi\begin{pmatrix} Q_1 \\ Q_2 \\ \vdots \\ Q_{N-1} \end{pmatrix} - \begin{pmatrix} Q_2 \\ Q_3 \\ \vdots \\ Q_N \end{pmatrix} = 0.$$

We use Newton's method to solve the above system. If $Q^{(j)} = \left(Q_1^{(j)}, Q_2^{(j)}, ..., Q_N^{(j)}\right)^T$, denotes the j-th iterate of the procedure, Newton's equations can be written as

$$DF(Q^{(j)}) \cdot (Q^{(j+1)} - Q^{(j)}) = -F(Q^{(j)}),$$

where the differential of the function F has the following structure

$$DF = \begin{pmatrix} A_1 & -I & & & \\ & A_2 & -I & & \\ & & \ddots & \ddots & \\ & & & A_{N-1} & -I \end{pmatrix},$$

with

$$D\Phi = \begin{pmatrix} A_1 & & & \\ & A_2 & & \\ & & \ddots & \\ & & & A_{N-1} \end{pmatrix}.$$

As each of the transition matrices, A_i, that appear in $D\Phi$ are 6×6, at each step of the method we have to solve a system of $(N-1) \times 6$ equations with $6 \times N$ unknowns, so some additional conditions must be added. This is the only difference with the standard multiple shooting method and is due to the fact that our problem is not a real boundary-value one. As additional equations we could fix some initial and final conditions at $t = t_0$ and $t = t_N$. This strategy has been used in [11] and [12] for the numerical refinement of halo orbits. In this case one must take care with the choice because the problem can be ill conditioned from the numerical point of view. This is because the matrix $DF(Q)$ has a very large condition number. If we assume that Δt is of the order of one revolution, all the matrices A_i are similar and if the largest eigenvalue is λ ($\simeq 1500$), the smallest is λ^{-1}, so the condition number is of the order of λ^2. To avoid this bad conditioning, we can choose a small value for Δt. In this case the largest eigenvalue of A_i is not so large, but as the number of points Q_i increases (if we want to cover the same time span) the instability is transfered to the procedure for solving the linear system. Also, the extra boundary conditions can force the solution in a non natural way giving convergence problems when we try to compute the orbit for a long time interval.

To avoid this, we can apply Newton's method directly. As the system has more unknowns than equations, we have (in general) an hyperplane of solutions. From this set of solutions we try to select the one closer to the initial orbit used to start the procedure. This is done by requiring the correction to be minimum with respect to some norm (i.e. the euclidean norm, see [36]). The use of the normal equations must be avoided because they are usually ill conditioned too. In our situation we have used the structure of the equations in the following way.

Denoting by $\Delta Q^{(j)}$

$$\Delta Q^{(j)} = Q^{(j+1)} - Q^{(j)},$$

if we require $\|\Delta Q^{(j)}\|_2$ to be minimum, using the Lagrange function $L(\Delta Q, \mu)$ with (vector) multiplier μ

$$L(\Delta Q, \mu) = \Delta Q^T \cdot \Delta Q + \mu^T \cdot (F(Q) + DF(Q) \cdot \Delta Q),$$

we get

$$\Delta Q^{(j)} = -DF(Q^{(j)})^T \cdot \left[DF(Q^{(j)}) \cdot DF(Q^{(j)})^T\right]^{-1} \cdot F(Q^{(j)}), \tag{14}$$

which gives the value of $\Delta Q^{(j)}$ explicitly. Let $M = DF(Q^{(j)}) \cdot DF(Q^{(j)})^T$. This is a symmetric band matrix with the following pattern

$$M = \begin{pmatrix} I + A_1 A_1^T & -A_1 & & & \\ -A_1^T & I + A_2 A_2^T & -A_2 & & \\ & \ddots & \ddots & \ddots & \\ & & -A_{N-3}^T & I + A_{N-2} A_{N-2}^T & -A_{N-2} \\ & & & -A_{N-2}^T & I + A_{N-1} A_{N-1}^T \end{pmatrix}.$$

We introduce additional variables, $Z^{(j)}$, by $M^{-1} F(Q^{(j)}) = Z^{(j)}$, and then equation (14) becomes

$$\begin{aligned} M \cdot Z^{(j)} &= F(Q^{(j)}), & (15)\\ \Delta Q^{(j)} &= -DF(Q^{(j)})^T \cdot Z^{(j)}. & (16) \end{aligned}$$

Now we use a block Cholesky factorization to express M as

$$\begin{pmatrix} I & & & \\ L_2 & I & & \\ & \ddots & \ddots & \\ & & L_{N-1} & I \end{pmatrix} \cdot \begin{pmatrix} D_1 & & & \\ & D_2 & & \\ & & \ddots & \\ & & & D_{N-1} \end{pmatrix} \cdot \begin{pmatrix} I & L_2^T & & \\ & \ddots & \ddots & \\ & & I & L_{N-1}^T \\ & & & I \end{pmatrix},$$

obtaining the following recursive relations

$$\begin{aligned} D_1 &= I + A_1 A_1^T, & \\ L_i &= -A_i D_{i-1}^{-1}, & i = 2, 3, ..., N-1, \\ D_i &= I + A_i A_i^T - L_i D_{i-1} L_i^T, & i = 2, 3, ..., N-1. \end{aligned}$$

With this factorization, system (15) can be solved recursively using intermediate variables, X, Y, with block components X_1,..., X_{N-1}, Y_1,...,Y_{N-1} such that $Y = Z^{(j)}$ and $F = (F_1, ..., F_{N-1})$

$$\begin{aligned} X_1 &= F_1(Q^{(j)}), & \\ X_k &= F_k(Q^{(j)}) - L_k X_{k-1}, & k = 2, 3, ..., N-1, \\ Y_{N-1} &= D_{N-1}^{-1} X_{N-1}, & \\ Y_k &= D_k^{-1} X_k - L_{k+1}^T Y_{k+1}, & k = N-2, N-3, ..., 1. \end{aligned}$$

The value of $\Delta Q^{(j)}$ can be computed using (16). From these last equations it is clear that the "dangerous" matrices are the D_k that appear in the recursive computation of X_k and Y_k. But now these matrices, if Δt is small, are close to diagonal matrices with all the diagonal elements close to $-1/2$, $-2/5$, $-5/12$, ... for $k = 2, 3, 4, \ldots$ respectively, so that they do not amplify the errors at each step of the procedure. Even if Δt is close to the time required for one revolution, the spectral radius of these matrices is close to one.

8 SOME NUMERICAL RESULTS

We have used the above results to produce orbits in the model of solar system given by the JPL ephemeris DE403. In order to illustrate the procedure we will first show the details of some iterations of the computation of a particular solution.

For this first example, to start the algorithm we use as initial nodes, Q_i, that is, the components of $Q^{(0)}$, points on a quasihalo orbit of the Sun–Earth+Moon system around the L_1 point with $\beta = 0.20$ and $\gamma = 0.08$. Note that this is beyond the values displayed in figures 16 and 17, but the shooting method will still be able to cope with this difficulty. We fix the initial epoch to be January 1 of the year 2000, and we use 40 nodes with a time step, Δt, between two consecutive ones of 180 days. This covers a total time span of 19.7 years. So, the total number of revolutions "around" the equilibrium point L_1 is approximately 39 and we have taken 1 point (approximately) on each revolution to perform the multiple shooting. In figure 18 we show the (x, y)

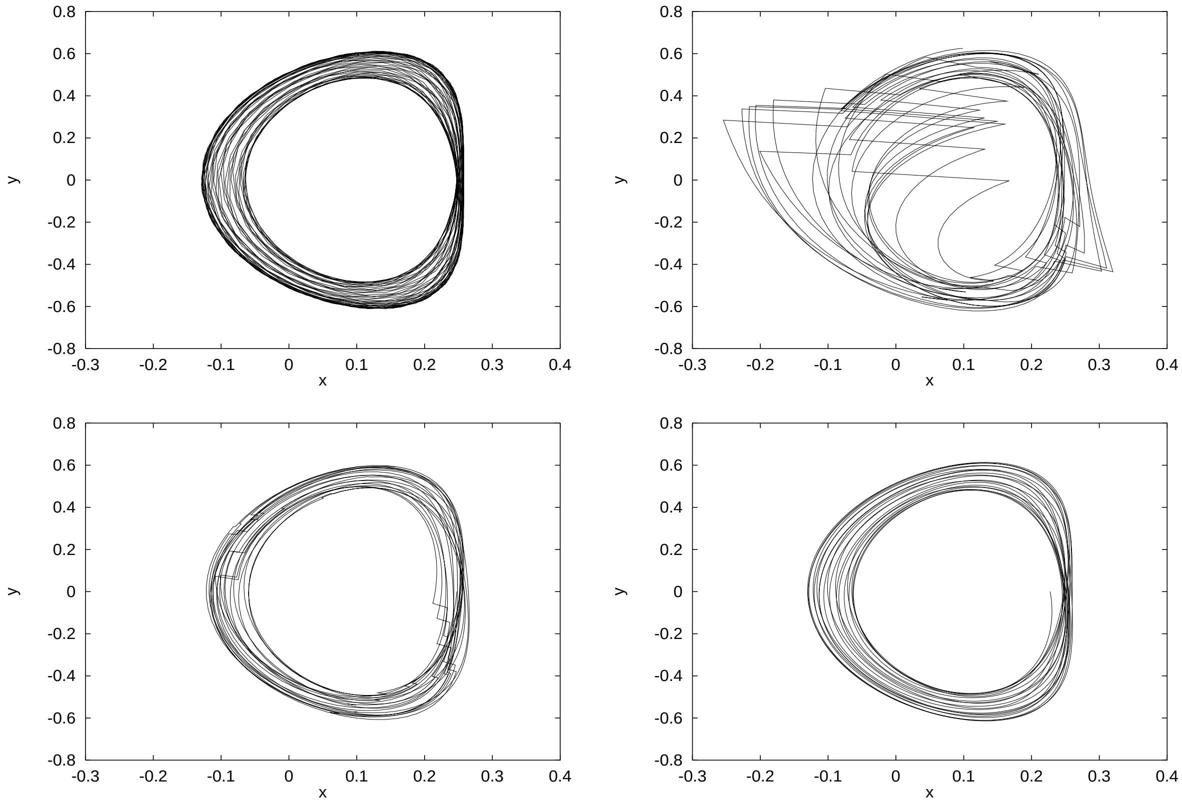

Figure 18: (x, y) projections of the orbits obtained with the multiple shooting procedure at different steps. The figure on the left upper corner is the orbit of the RTBP, computed with the expansions, from which the initial points Q_i are taken. The orbits with large jumps discontinuities are the ones obtained after the first two iterations. The figure on the right lower corner is the orbit computed after 8 iterations. The initial orbit is a quasihalo orbit with $\beta = 0.2$ and $\gamma = 0.08$.

projection of the orbit after different iterations of the procedure. All the figures are represented in normalized coordinates centered at the L_1 point. The first plot corresponds to the orbit, computed with the analytical expansions, from where the points Q_i were taken. It is an approximate solution (due to the truncation and asymptotic character of the series) of the RTBP equations of motion. The next two, showing large discontinuities at some points, are the results obtained after the first two iterations. The different pieces that constitute the orbit do not match at the nodes in these first steps because the initial conditions were taken from a solution of the RTBP and now we are integrating these initial conditions in a model including all the bodies of the solar system with its real motion. These discontinuities are so large because of the highly unstable character of the solution. The last plot corresponds to the orbit computed after 8 iterations. The discontinuities that appear in the first iterations are reduced to "zero" by the method. In the first step, adding the corrections applied at all the nodes, the total correction in position ($|\Delta Q^{(0)}_{1,2,3}|_2 + |\Delta Q^{(0)}_{7,8,9}|_2 + ...$) is of 319600.6 km and of 9360.6 km/day in velocity, which means an average value for the corrections at each point of 8000 km and 235 km/day. After eight iterations the total amount of the corrections has been reduced to 37 mm and less than 1 mm/day, for positions and velocities, respectively. Taking shorter time intervals between consecutive nodes, the norm of the function F is much smaller at the first steps and the number of Newton iterations decreases. For the Sun–Earth+Moon system, a value of Δt equal to 7 days requires no more than 4 or 5 iterations to get a final solution with discontinuities at the nodes smaller than tracking errors. For the Earth–Moon system, the computations must be done more carefully and a time step of 1/2 day has given good results.

#	Position (Km)	Velocity (Km/day)
1	0.1173580E+07	0.5122975E+05
2	0.1342529E+06	0.6721532E+04
3	0.9088254E+05	0.4065216E+04
4	0.8446439E+03	0.4352568E+02
5	0.5525061E+02	0.2369489E+01
6	0.3735932E−03	0.2989727E−04
7	0.1056651E−04	0.5026301E−06
8	0.3753297E−05	0.1723968E−06

Table 2: Euclidean norm of the function F evaluated at the nodes at the first 8 steps of the multiple shooting. In the second column the norm of the first three components of F is given (error in position) and in the second for the last three ones (error in velocity).

Table 2 gives the values of the function $\|F(Q_1^{(j)}, Q_2^{(j)}, ..., Q_{40}^{(j)})\|_2$ at the different steps of the algorithm. We have separated the components in position from the ones in velocity. After the iteration number 8 no further inprovement is achieved.

We have done many refinements of quasihalo orbits in all the situations. For the Sun–Earth+Moon system the refinement can be done without any problem for all kinds of orbits and for very large time spans (almost all the refined orbits that we have computed cover a time interval of 20 years). In the Earth–Moon system the situation is not so nice. The refinements can also be done without any problem for a time interval of 6–8 years. For larger intervals the procedure must be modified slightly. This is done by requiring to the norm of the correction, $\|\Delta Q^{(j)}\|_2$, to be minimum for a reduced set of nodal points and at the other nodes computing the correction without any constrain (see [1] for the details and [2] for an illustration). Also the time step between two consecutive nodes must be shorter, between 1/2 and 1 day to get a satisfactory solution with few iterates.

As a test for the robustness of the method we have done the following experiment. As we have seen in a previous section, for a given value of the z–amplitude β, there is a maximum amplitude, γ, of the quasiperiodic orbits that can be reached with the analytical expansions computed. Some of these invariant tori, that almost foliate the phase space when we compute them up to a given order, do not exist for the RTBP due to the resonances that destroy them (or they exist, as suggested by computation on the center manifold, but the LP procedure is unable to provide good approximations). On the other hand it may happen that for these more realistic equations of motion, there exist these kind of quasihalo orbits with an amplitude larger than the maximum one obtained using the asymptotic expansions. For this maximum we have done (in section 6) two estimates: one comparing the expansions with the direct numerical computation and the other estimating the residual acceleration; here we have taken the most pessimistic of both estimates as practical convergence radii, that is, the minimum of the values plotted in figure 16 and figure 17, using in last one the value 10^{-6} for the threshold. We have used values of γ larger than this maximum to compute the nodes, Q_i, as initial points to start the multiple shooting procedure. For all the situations explored we have been able to go beyond the maximum value of γ given by the radius of convergence, and to obtain solutions of the real system which look like quasiperiodic halo orbits. In table 3 we give, for different values of β, the values of the practical convergence radii and the maximum value of γ reached (using a rough step of 0.005 in γ), both for the L_1 and L_2 points of the Sun–Earth+Moon system. All the orbits were computed for a total time span of 7000 days (approximately 19 years) starting at January 1 of the year 2000. Similar results, but for the Earth–Moon system are given in table 4, where the time span has been taken of 2000 days.

	L_1		L_2	
β	Practical convergence radii	Maximum γ	Practical convergence radii	Maximum γ
0.05	0.015	0.035	0.023	0.050
0.10	0.029	0.065	0.043	0.085
0.15	0.043	0.090	0.061	0.125
0.20	0.056	0.105	0.079	0.165
0.25	0.068	0.145	0.093	0.200

Table 3: For different values of β, values of the minimum practical radii of convergence estimated (see section 6) of the quasihalo orbits expansions and the maximum amplitude reached in the refinement of these orbits. The results correspond to the Sun–Earth+Moon system.

	L_1		L_2	
β	Practical convergence radii	Maximum γ	Practical convergence radii	Maximum γ
0.05	0.015	0.025	0.044	0.060
0.10	0.029	0.045	0.081	0.085
0.15	0.042	0.060	0.075	0.075
0.20	0.056	0.065	0.052	0.065
0.25	0.069	0.080	0.033	0.050

Table 4: Same as table 3 but for the Earth–Moon system.

As a sample of the results obtained, in figures 19, 20, 21 and 22 we show some of these orbits for the maximum values of γ reached for the four different situations explored. In each of the figures on the left hand side we plot the "pseudo-orbits", computed with the divergent expansions (where the initial points are taken from) and on the right hand side, the final refined orbits.

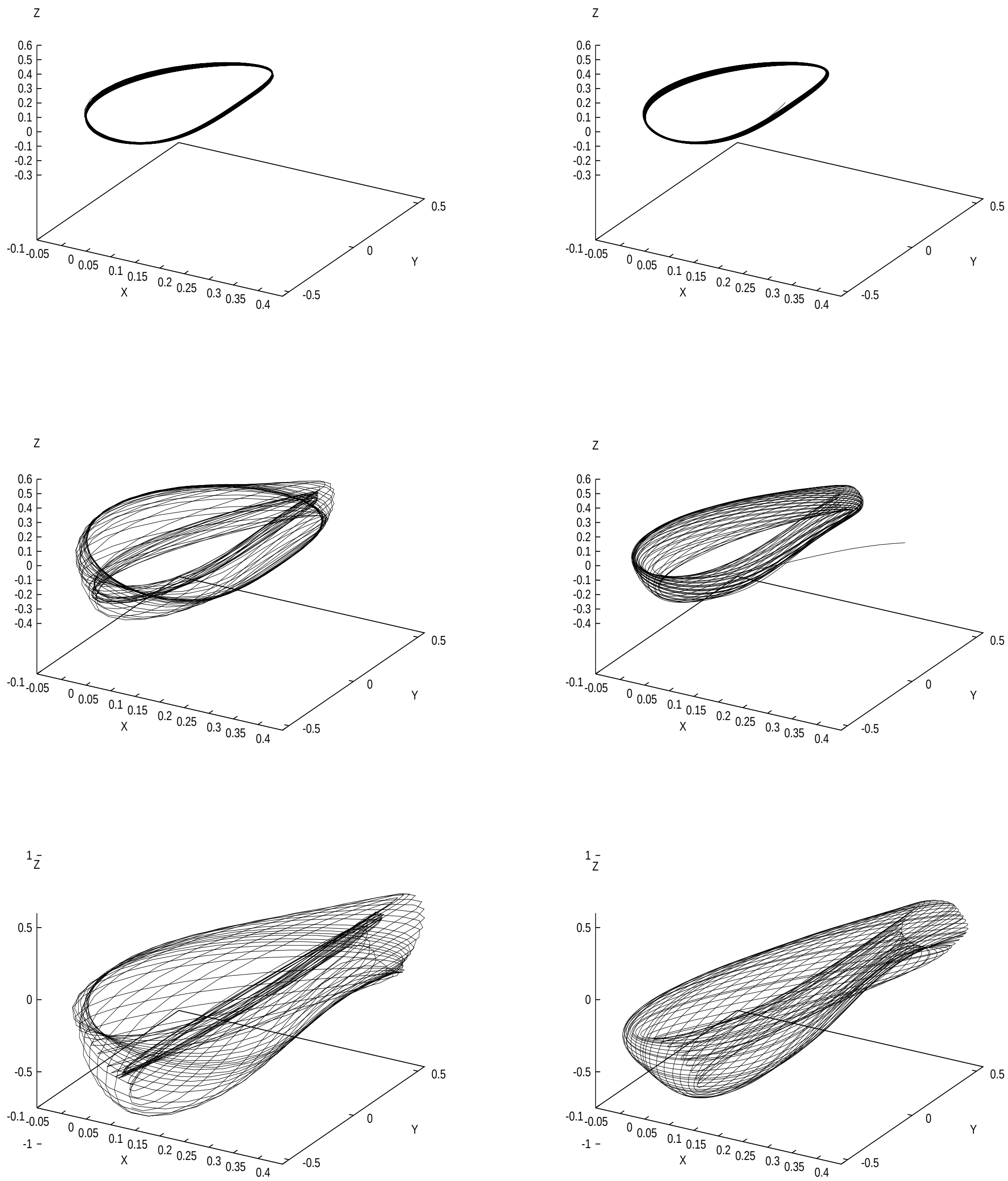

Figure 19: Refinements of quasihalo orbits with γ amplitudes out of the region of convergence of the expansions. In the left figures we plot the quasiperiodic formal "solution" on which the initial points are taken. In the right figures the refined orbits have been represented. From top to bottom, the orbits correspond to values of β and γ equal to (0.05, 0.035), (0.15, 0.090) and (0.25, 0.145) respectively. All the orbits are in the Sun–Earth+Moon system around the L_1 point. Note that the initial and final arcs of the numerically computed orbit can go away from a motion looking like quasiperiodic.

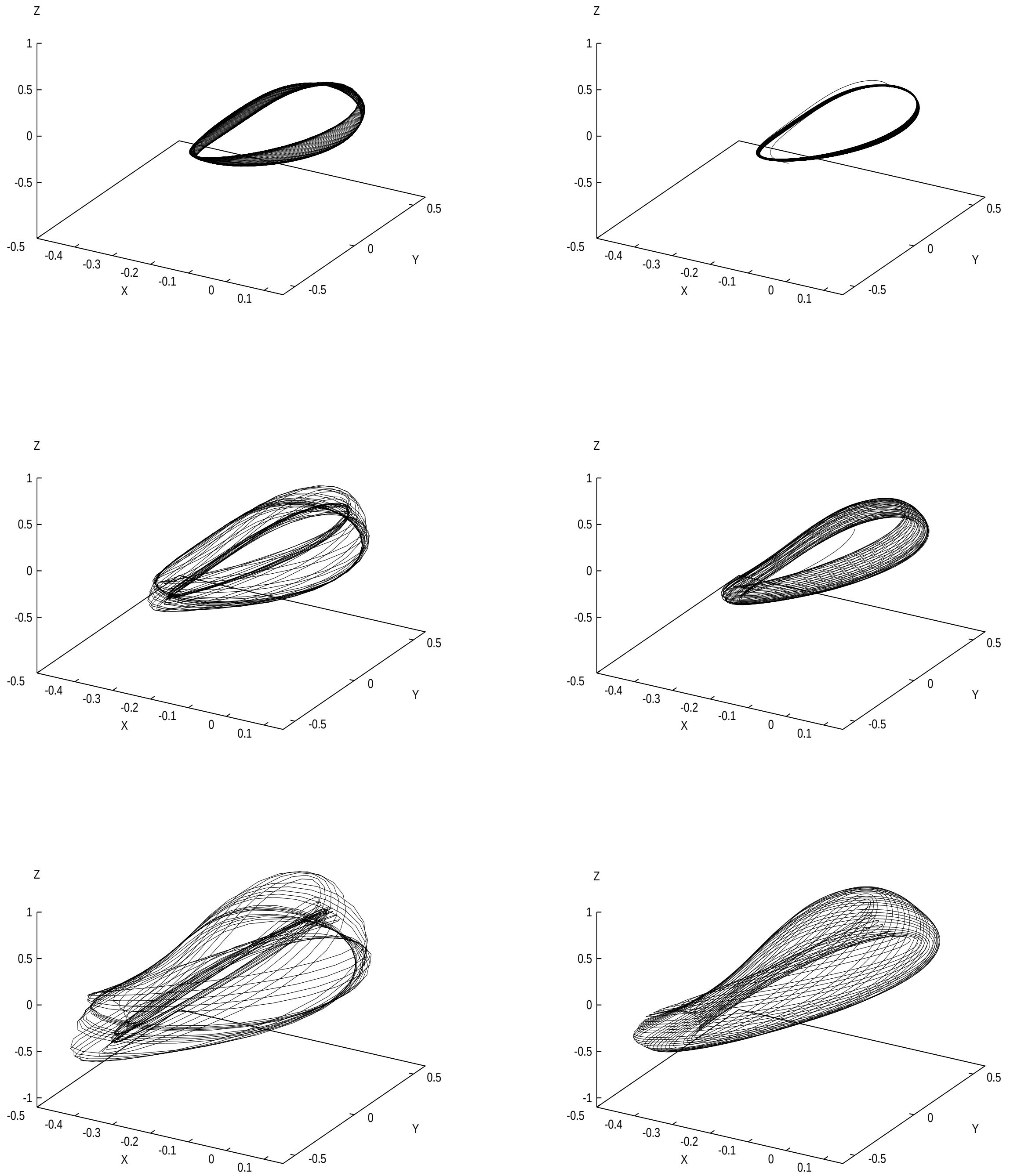

Figure 20: Same as figure 19 but for the L_2 point. From top to bottom, the orbits correspond to values of β and γ equal to (0.05, 0.050), (0.15, 0.125) and (0.25, 0.200) respectively.

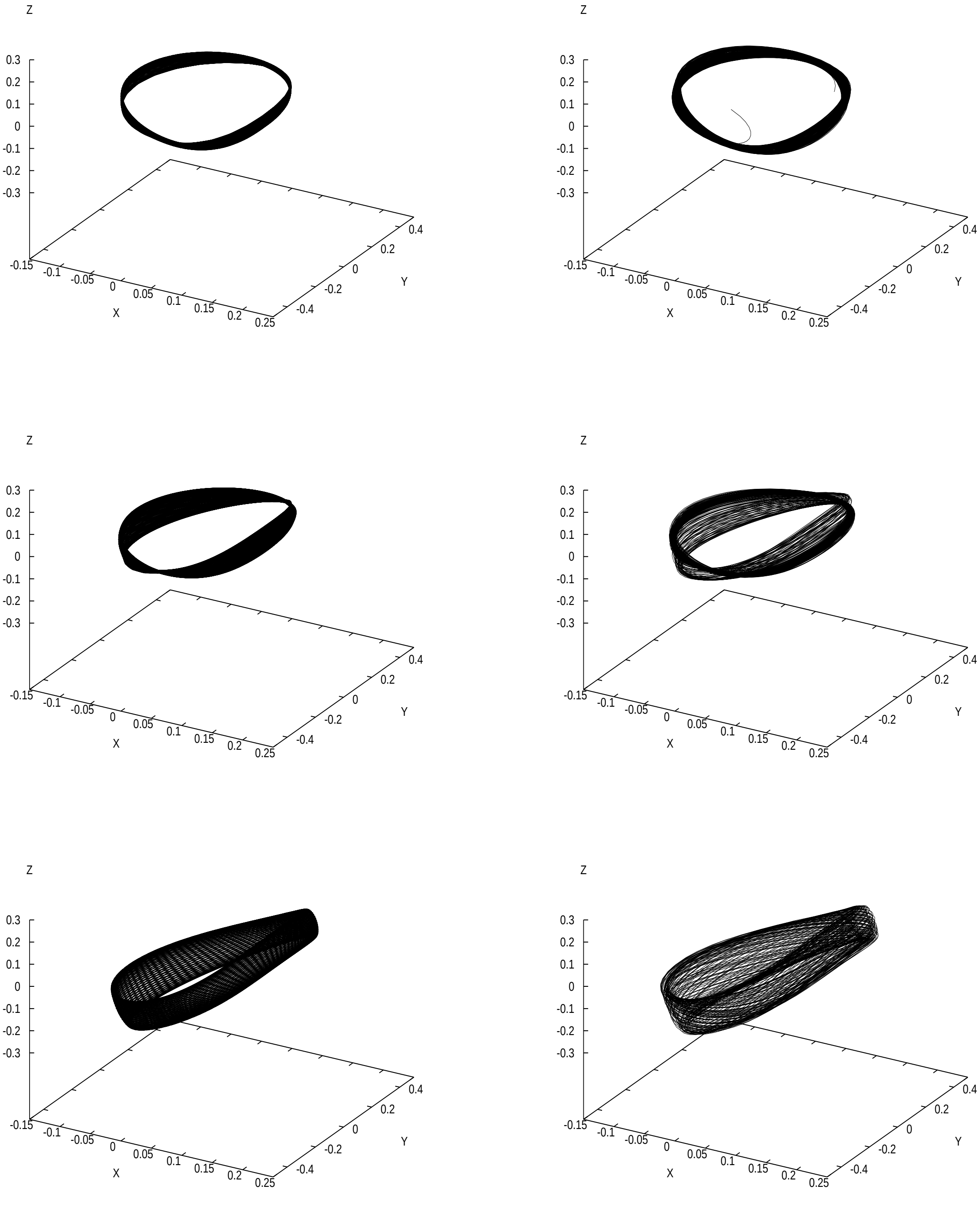

Figure 21: Same as figure 19 but for the Earth–Moon system L_1 point. From top to bottom, the orbits correspond to values of β and γ equal to (0.05, 0.025), (0.15, 0.060) and (0.25, 0.080) respectively.

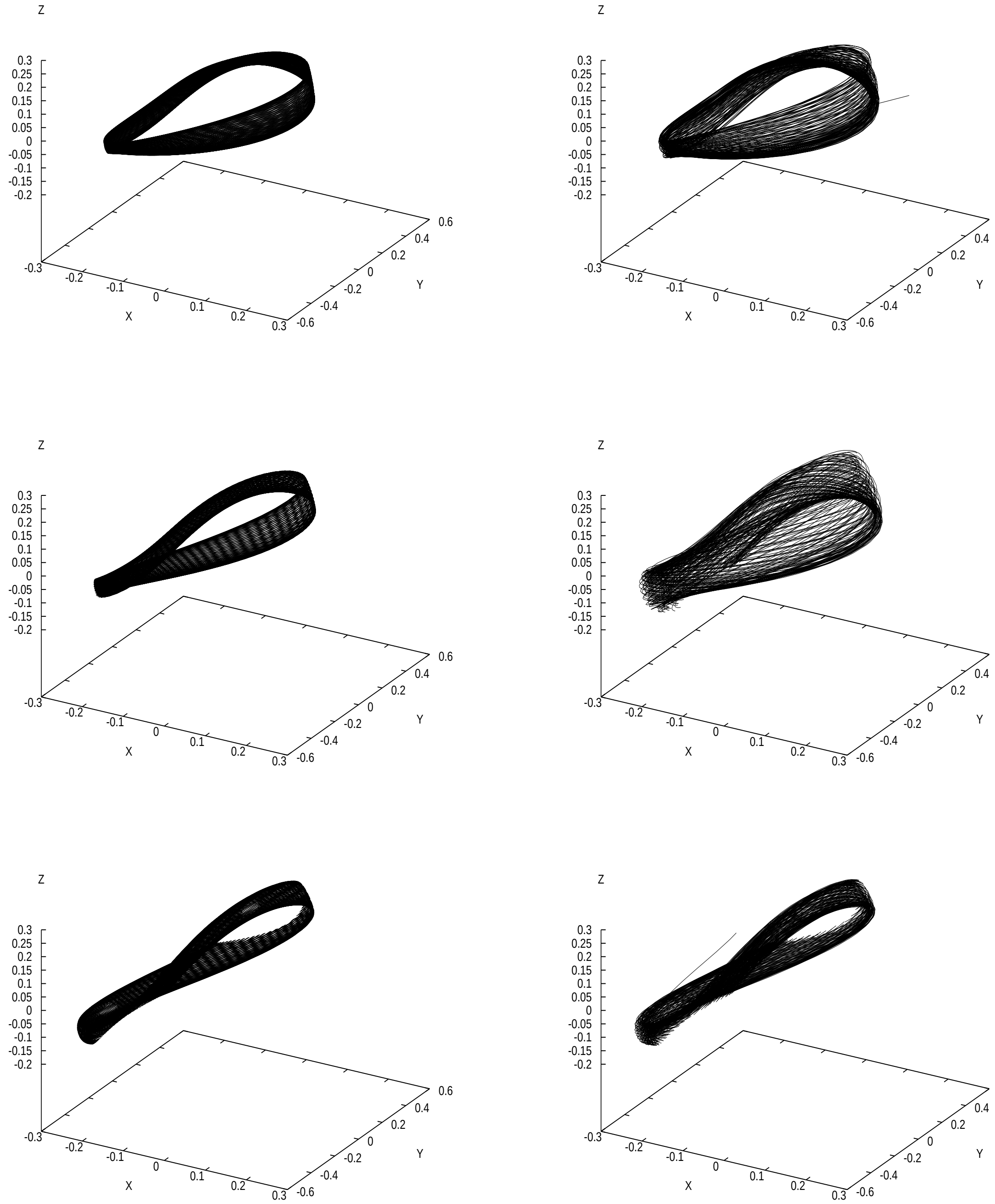

Figure 22: Same as figure 19 but for the Earth–Moon system L_2 point. From top to bottom, the orbits correspond to values of β and γ equal to (0.05, 0.065), (0.15, 0.075) and (0.25, 0.050) respectively.

Note that, due to weak conditions imposed in the multiple shooting procedure, the initial and final arcs of the displayed orbits can go away from a motion looking like quasiperiodic. Indeed, no conditions are imposed on the end points. So, in general, most of the computed orbits are very close to an unstable torus (assuming it exists!) except for the initial arc, close to its stable manifold, and the final arc, close to the unstable one. The large value of the Lyapunov number ensures that these two arcs can be visible for, at most, one “revolution”.

Another point worth to be mentioned is the exceptional behaviour of the quasihalo orbits in the L_2 Earth–Moon case when the full solar system is considered. Looking to figures 19, 20 and 21, the tori become thicker from top to bottom, in correspondence with an increase of the amplitudes. The situation is different in figure 22, where the thickest torus appears in the middle plot. Of course, both amplitudes β and γ play a role, but there is also a strong effect due to the 2:1 resonance between the frequency of the halo orbit and the synodical frequency of the Sun in the Earth–Moon system (see [1] for details). This do not happens in the L_1 Earth–Moon case.

9 CONCLUSIONS

A method to compute Lissajous orbits around the halo orbits near the collinear libration points in the RTBP has been introduced. It is based on a variant of the classical Lindstedt-Poincaré method. The full procedure is given in detail. To demonstrate the feasibility, the required symbolic manipulation software has been developed, implemented and run on several examples. Exhaustive tests concerning the domain of applicability and direct numerical verifications have been done, as well as the numerical extensions when the full solar system is considered. We can conclude that a new methodology is available to enlarge the set of candidates of nominal orbits ready to be used for future space missions in an extended vicinity of the collinear libration points associated with any three body system.

10 Acknowledgements:

This work has been supported by DGICYT Grant PB 94–0215 (Spain). Partial support of the EC grant ERBCHRXCT 940460, and the catalan grant CIRIT 1996S0GR-00105 is also acknowledged. We thank À. Jorba for many helpful discussions, and the (unknown) referees for careful reading and many suggestions allowing us to improve the readibility of the paper.

References

[1] Andreu, M.A.: *The Quasibicircular Problem*, Ph. D. Thesis, Dept. Matemàtica Aplicada i Anàlisi, Universitat de Barcelona, 1998.

[2] Andreu, M.A., Simó, C.: Translunar Halo Orbits in the Quasibicircular Model. To appear in *The Dynamics of Small Bodies in the Solar System*, Proceed. NATO ASI, Maratea (Italy), ed. A. Roy, 1998.

[3] Breakwell, J.V., Kamel, A.A., Ratner, M.J.: Station–Keeping for a Translunar Communications Station. *Celestial Mechanics*, Vol 10 (1974) 357–373.

[4] Broer, H., Simó, C.: Resonance tongues in Hill's equations: a geometric approach. Preprint, 1997.

[5] Broer, H., Simó, C., Tatjer, J.C.: Towards global models near homoclinic tangencies of dissipative diffeomorphisms. *Nonlinearity*, Vol 11 (1998) 667–770.

[6] Coddington E.A., Levinson N., *Theory of Ordinary Differential Equations*, Mc Graw-Hill, New York 1955.

[7] Farquhar, R.W.: Halo-Orbit and Lunar-Swingby Missions of the 1990's. *Acta Astronautica*, Vol 24 (1991) 227–234.

[8] Farquhar, R.W., Kamel, A.A.: Quasi-Periodic Orbits about the Translunar Libration point. *Celestial Mechanics*, Vol 7 (1973) 458–473.

[9] Farquhar, R.W., Muhonen, D.P., Newman, C., Heuberger, H.: The first libration point satellite. Mission overview and flight history. AAS/AIAA Astrodynamics Spec. Conf., 1979.

[10] Giacaglia, G.E.O.:*Perturbation Methods in non–linear Systems*, Springer–Verlag, 1972.

[11] Gómez, G., Llibre, J., Martínez, R., Simó, C.: Station Keeping of Libration Point Orbits, ESOC Contract 5648/83/D/JS(SC), Final Report, 1985.

[12] Gómez, G., Jorba, À., Masdemont, J., Simó, C.: Study Refinement of Semi-Analytical Halo Orbit Theory. ESOC Contract 8625/89/D/MD(SC), Final Report, 1991.

[13] Gómez, G., Jorba, À., Masdemont, J., Simó, C.: Moon's influence on the transfer from the Earth to a Halo orbit. *Predictability, Stability and Chaos in N-Body Dynamical Systems.* Ed. A. E. Roy. Plenum Press 1991, 283–290.

[14] Gómez, G., Jorba, À., Masdemont, J., Simó, C.: A Dynamical Systems Approach for the Analysis of the SOHO Mission, *Proc. Third Int. Symp. Spacecraft Flight Dynamics* ESA SP-326 (1991) 449-454.

[15] Gómez, G., Jorba, À., Masdemont, J., Simó, C.: Study of the Transfer from the Earth to a Halo Orbit around the Equilibrium Point L_1. *Celestial Mechanics*, Vol 56 (1993) 541–562.

[16] Gómez, G., Masdemont, J., Simó, C.: Lissajous Orbits around Halo orbits. AAS Paper 97–106. *Advances in the Astronautical Sciences*, Vol 95 (1997) 117–134.

[17] Goudas, C.L.: Three dimensional periodic orbits and their stability, *Icarus*, Vol 2 (1963) 1–18.

[18] Hénon, M.: Vertical stability of periodic orbits in the restricted problem I. Equal masses, *Astronomy & Astrophysics*, Vol 28 (1973) 415–426.

[19] Howell, K.C., Barden, B.T., Wilson, R.S., Lo, M.W.: Trajectory Design Using a Dynamical Systems Approach with Application to Genesis. AAS Paper 97-709. AAS/AIAA Astrodynamics Specialist Conference, Sun Valley, Idaho, 1997.

[20] Howell, K.C., Gordon, S.C.: Orbit Determination Error Analysis and a Station–Keeping Strategy for Sun–Earth L_1 Libration Point Orbits. *Journal of the Astronautical Sciences*, Vol 42 (1994) 207–228.

[21] Howell, K.C., Pernicka H.J.: Numerical Determination of Lissajous Trajectories in the Restricted Three-Body Problem. *Celestial Mechanics*, Vol 41 (1988) 107–124.

[22] Howell, K.C., Pernicka H.J.: Stationkeeping Method for Libration Point Trajectories. *Journal of Guidance, Control, and Dynamics*, Vol 16 (1980) 549–554.

[23] Huber, M.C.E. et al.: The History of the SOHO Mission. *ESA Bulletin*, Vol 86 (1996) 25–35.

[24] Jorba, À., Masdemont, J., Nonlinear Dynamics in an Extended Neighbourhood of the Translunar Equilibrium Point, in *NATO–ASI Hamiltonian Systems with Three or More Degrees of Freedom*, eds. C. Simó, A. Delshams.

[25] Jorba, À., Simó, C.: On Quasiperiodic Perturbations of Elliptic Equilibrium Points, *SIAM J. of Math. Analysis*, Vol27 (1996) 1704–1737.

[26] Jorba, À., Villanueva, J.,: On the Normal Behaviour of Partially Elliptic Lower Dimensional Tori of Hamiltonian Systems, *Nonlinearity*, Vol 10 (1997) 783–822.

[27] Jorba, À., Villanueva, J.: On the Persistence of Lower Dimensional Invariant Tori under Quasiperiodic Perturbations, *J. Nonlinear Science*, Vol 7 (1997) 427–473.

[28] Jorba, À., Villanueva, J.,: Numerical Computation of Normal Forms Around Some Periodic Orbits of the Restricted Three Body Problem. *Physica* **D**, Vol 114 (1998) 197–229.

[29] Poincaré, H.: *Les Méthodes Nouvelles de la Mécanique Céleste*, Gauthier–Villars, 1892, 1893, 1899.

[30] Richardson, D.L.: A Note on the Lagrangian Formulation for Motion About the Collinear Points, *Celestial Mechanics*, Vol 22 (1980) 231-236.

[31] Richardson, D.L.: Analytical construction of periodic orbits about the collinear points. *Celestial Mechanics*, Vol 22 (1980) 241–253.

[32] Richardson, D.L.: Halo orbit formulation for the ISEE-3 mission. *J. Guidance and control*, Vol 3 (1980) 543–548.

[33] Richardson, D.L., Cary N.D.: A Uniformly Valid Solution for Motion About the Interior Libration Point of the Perturbed Elliptic-Restricted Problem. AAS Paper 75-021. AAS/AIAA Astrodynamics Specialist Conference. Nassau, Bahamas. July 1975.

[34] Rodríguez-Canabal J.: Operational Halo Orbit Maintenance Technique for SOHO. *Second International Symposium on Spacecraft Flight Dynamics* ESA SP–255 (1986) 71–78.

[35] Sharer, P., Zsoldos, J., Folta, D.: Control of Libration Point Orbits using Lunar Gravity-Assisted Transfer. AAS Paper 93–295. *Advances in the Astronautical Sciences*, Vol 84 (1993) 651–663.

[36] Simó, C.: Analytical and numerical computation of invariant manifolds, in *Modern methods in Celestial Mechanics*, D. Benest and C. Froeschlé, editors, pp. 285–330, Editions Frontières, 1990.

[37] Simó, C.: Effective Computations in Hamiltonian Dynamics, in *Cent ans après les Méthodes Nouvelles de H. Poincaré*, Société Mathématique de France, (1996) 1–23.

[38] Stoer, J., Burlirsch, R.:*Introduction to Numerical Analysis*, Springer Verlag, 1983.

[39] Zagouras, C.G., Kazantzis, P.G.: Three-dimensional periodic oscillations generating from plane periodic ones around the collinear Lagrangian points, *Astroph. Space Science* 61 (1979) 389–409.